BeFo

STIFTELSEN BERGTEKNISK FORSKNING
ROCK ENGINEERING RESEARCH FOUNDATION

STRUCTURAL BEHAVIOUR OF SHOTCRETE IN HARD ROCK TUNNELS

Andreas Sjölander

BeFo Report 210

STIFTELSEN BERGTEKNISK FORSKNING
ROCK ENGINEERING RESEARCH FOUNDATION

STRUCTURAL BEHAVIOUR OF SHOTCRETE IN HARD ROCK TUNNELS

Sprutbetongens verkningssätt i tunnlar i hårt berg

Andreas Sjölander, KTH Royal Institute of Technology

BeFo Report 210
Stockholm 2020
ISSN 1104-1773
ISRN BEFO-R-210-SE

This report is an adjusted version of the doctoral thesis "Structural behaviour of shotcrete in hard rock tunnels", which was defended at KTH Royal Institute of Technology on 4 June 2020.

Preface

Since the 1980's, tunnels in hard rock have predominately been supported by fibre-reinforced shotcrete in combination with rock bolts. This type of rock support is a complex composite structure in which the structural behaviour depends on the interaction between shotcrete, rock and bolts. Moreover, it is difficult to assess the mechanical properties and structural behaviour of the rock mass, which makes it difficult to predict the loads acting on the support system. The design is commonly based on a rock mass classification system in combination with analytical solutions or finite element modelling. In such case, the in-situ variations of shotcrete thickness and bond strength are normally neglected. Previous research has shown that relatively large in-situ variations of these parameters are expected. However, if and how this affect the structural capacity of the shotcrete is not clear.

The focus of this project was to describe and explain how the variations in shotcrete thickness and bond strength affect the structural behaviour and capacity for a shotcrete lining. Especially, the influence of local variations in shotcrete thickness and bond strength has been studied in detail. For this purpose, a numerical framework capable of simulating bond failure, cracking of FRS and pull-out failure of grouted rock bolts have been developed. Moreover, in-situ data for shotcrete thickness and bond strength have been collected and analysed to characterize the variations in important shotcrete parameters.

The research presented in this report is a summary of a Ph.D project carried out at KTH Royal Institute of Technology and the Division of Concrete Structures by Andreas Sjölander. Main supervisor for the project was Anders Ansell and co-supervisor was Richard Malm and Fredrik Johansson at the Division of Soil and Rock Mechanics. The reference group to this project has contributed with thoughtful advice and consisted of: Tommy Elisson (BESAB), Henrik Ittner (Theta Engineering), Mattias Roslin (Theta Engineering), Rikard Gothäll (Tyréns), Hans-Åke Mattson (AFRY), Lars Malmgren (LKAB) and Per Tengborg (BeFo). The project was funded by Rock Engineering Research Foundation (BeFo) and by the Construction Industry's Organisation for Research and Development (SBUF)

Stockholm, 2020

Per Tengborg

Förord

Sedan början av 1980-talet har fiberarmerad sprutbetong i kombination med bergbultar varit den dominerande bergförstärkningen för tunnlar i hårt berg. Den här typen av förstärkning är en komplex samverkanskonstruktion vars strukturella beteende styrs av interaktionen mellan sprutbetong, berg och bult. Dessutom är det svårt att bedöma bergets mekaniska egenskaper och deformation vilket gör det komplicerat att förutse vilka laster som bergförstärkningen ska dimensioneras för. Bergförstärkningar dimensioneras därför ofta baserat på ett klassificeringssystem för bergmassan i kombination med analytiska lösningar eller modeller baserade på finita elementmetoden. I dessa fall bortser man oftast från de i fält förekommande variationerna hos sprutbetongens viktiga egenskaper som t.ex. tjocklek och vidhäftningshållfasthet. Tidigare forskning har visat att relativt stora variationer i dessa parametrar existerar men det är inte klarlagt hur detta påverkar förstärkningens kapacitet.

Fokusområdet för detta forskningsprojektet var att förklara och beskriva hur variationerna i sprutbetongens tjocklek och vidhäftning påverkar det strukturella beteendet och bärförmågan hos bergförstärkningen. Framförallt har lokala variationer i sprutbetongens tjocklek och vidhäftning studerats. För att genomföra detta har ett numeriskt ramverk utvecklats som kan simulera uppsprickning av fiberarmerad sprutbetong, vidhäftningsbrott och utdrag av ingjutna bergbultar. Dessutom har fältdata samlats in och analyserats för att karaktärisera fördelningen av viktiga sprutbetongegenskaper.

Forskningen har utförts som ett doktorandprojekt på KTH avdelningen för betongbyggnad av Andreas Sjölander. Huvudhandledare för projektet har varit Anders Ansell och biträdande handledare har varit Richard Malm och Fredrik Johannson vid avdelningen för jord- och bergmekanik. Forskningsprojektets referensgrupp har bidragit under genomförandet med råd och granskning och bestod av: Tommy Ellison (BESAB), Henrik Ittner (Theta Engineering), Mattias Roslin (Theta Engineering), Rikard Gothäll (Tyréns), Hans-Åke Mattson (AFRY), Lars Malmgren (LKAB) och Per Tengborg (BeFo). Projektet har finansierats av Stiftelsen Bergteknisk Forskning (BeFo) och Svenska Byggbranschens Utvecklingsfond SBUF.

Stockholm, 2020

Per Tengborg

Abstract

Tunnels in hard and jointed rock are normally excavated in an arch shape to enable the rock mass to support its weight. Since the beginning of the 1980's, fibre reinforced shotcrete (FRS) in combination with rock bolts have been the dominating support method for hard rock tunnels. This type of rock support is a complex composite structure in which the structural behaviour depends on interaction between shotcrete, rock and bolts. The design is commonly based on a rock mass classification system in combination with analytical solutions or finite element (FE) modelling. However, the in-situ variations of important properties of the shotcrete are normally neglected.

The aim of this thesis is to describe and explain how the variations in shotcrete thickness and bond strength affect the structural behaviour and capacity for a shotcrete lining. Especially, the influence of local variations in shotcrete thickness and bond strength has been studied in detail. For this purpose, a numerical framework capable of simulating bond failure, cracking of FRS and pull-out failure of grouted rock bolts have been developed. Moreover, in-situ data for shotcrete thickness and bond strength have been collected and analysed to characterize the variations in important shotcrete parameters.

The results in this thesis show that when shotcrete is subjected to shrinkage, local variations in shotcrete thickness affects the crack pattern. However, the number and width of the cracks are similar to the case with uniform thickness. Most importantly, a pattern of fine and narrow cracks develops in unreinforced shotcrete subjected to shrinkage when a continuous bond to the rock exists. When shotcrete is subjected to the load from a loose block, the force is transferred to the surrounding rock through bond stresses distributed over a narrow band. Simulations have shown that the structural capacity, with respect to bond failure, depends on the shotcrete thickness. Moreover, a strong linear correlation was found between the mean value of the bond strength and shotcrete thickness around the perimeter of the block and the structural capacity. Local weak areas, i.e. with low bond strength or thickness, may exist around the perimeter without having a significant effect on the structural capacity. Design of bolt-anchored shotcrete linings is based on failure modes previously derived from experimental testing. This thesis has contributed to an increased understanding of the failure mechanisms of the lining and has confirmed that the design can be based on individual failure mechanisms.

Sammanfattning

Sedan början av 1980-talet har stålfiberarmerad sprutbetong i kombination med bergbultar varit den dominerande bergförstärkningen för tunnlar i hårt berg. Den här typen av förstärkning är en komplex samverkanskonstruktion vars strukturella beteende styrs av interaktionen mellan sprutbetong, berg och bult. Dimensioneringen baseras vanligtvis på ett klassificeringssystem för bergmassan i kombination med analytiska lösningar eller modeller baserade på finita elementmetoden. I dessa fall bortser man oftast från de i fält förekommande variationerna hos sprutbetongens viktiga egenskaper.

Syftet med denna avhandling är förklara och beskriva hur variationerna i sprutbetongens tjocklek och vidhäftning påverkar det strukturella beteendet och bärförmågan hos bergförstärkningen. Framförallt har lokala variationer i sprutbetongens tjocklek och vidhäftning studerats. För att genomföra detta har ett numeriskt ramverk utvecklats som kan simulera uppsprickning av fiberarmerad sprutbetong, vidhäftningsbrott och utdrag av injekterade bergbultar. Dessutom har fältdata samlats in och analyserats för att karaktärisera fördelningen av viktiga sprutbetongegenskaper.

Resultaten i den här avhandlingen visar att lokala variationer i sprutbetongens tjocklek påverkar sprickmönstret när sprutbetongen krymper. Antalet sprickor och dess vidd är liknande dem som uppstår när tjockleken är jämn. En viktig slutsats är att ett många sprickor med liten sprickvidd uppstår när oarmerad sprutbetong med kontinuerlig vidhäftning till berget krymper. När sprutbetongen utsätts för lasten från ett löst bergblock överförs lasten till den omkringliggande bergmassan längs ett tunt band. Numeriska simuleringar har visat att bärförmågan med avseende på vidhäftningsbrott beror på sprutbetongens tjocklek.

Dessutom visade simuleringarna att det finns ett starkt linjärt samband mellan medelvärdet för sprutbetongens tjocklek och vidhäftningshållfasthet längs blockets periferi och dess bärförmåga. Lokala ytor med liten tjocklek eller vidhäftningshållfasthet kan finnas runt periferin utan att påverka bärförmågan. Dimensioneringen av bultförankrad sprutbetong är baserad på brottmoder framtagna utifrån experiment. Den här avhandlingen har bidragit med en ökad förståelse kring dessa brottmoder och visat att dimensioneringen bör baseras på individuella brottmoder.

List of Publications

Below is a list of publications produced within this research project presented.

A. Sjölander, T. Gasch, A. Ansell and R. Malm. Shrinkage cracking of thin irregular shotcrete shells using multiphysics models. *Proceedings of the 9th International Conference on Fracture Mechanics of Concrete and Concrete Structures.* Berkeley, USA, May 2016.

A. Sjölander and A. Ansell. Numerical simulations of restrained shrinkage cracking in glass fibre reinforced shotcrete slabs. *Advances in Civil Engineering*, pp 1-11, 2017.

A. Sjölander, W. Bjureland and A. Ansell. On failure probability of thin irregular shotcrete shells. *Proceedings of ITA-AITES World Tunnel Conference 9.* Bergen, Norway, June 2017.

L. Ahmed, A. Sjölander and A. Ansell. Evaluation and analysis of laboratory tests of bolt-anchored, steel-fibre-reinforced shotcrete linings. *Proceedings of ITA-AITES World Tunnel Conference 9.* Bergen, Norway, June 2017.

A. Sjölander and A. Ansell. Analysis of the interaction between rock and shotcrete for tunnel support. *Proceedings of XXIII Nordic Concrete Research Symposium.*Aalborg, Denmark, August 2017.

A. Sjölander. *Analyses of shotcrete stress states due to varying lining thickness and irregular rock surfaces.* Licentiate thesis. KTH Royal Institute of Technology. Stockholm, Sweden, 2017.

A. Sjölander and A. Ansell. Investigation of non-linear drying shrinkage for end-restrained shotcrete with varying thickness. *Magazine of Concrete Research*, 70, pp 271-279, 2018.

A. Sjölander, R. Hellgren and A. Ansell. Modelling aspects to predict failure of a bolt-anchored and fibre reinforced shotcrete lining. *Eight International Symposium on Sprayed Concrete.* Trondheim, Norway, June 2018.

W. Bjureland, F. Johansson, A. Sjölander, J. Spross, and S. Larsson. Probability distributions of shotcrete parameters for reliability-based analyses of rock tunnel support. *Tunnelling and Underground Space Technology*, 87, pp 15-26, 2019.

A. Sjölander and A. Ansell. Probabilistic modelling of fibre reinforced shotcrete. *Proceedings of ITA-AITES World Tunnel Conference 10.* Naples, Italy, May 2019.

A. Sjölander and A. Ansell. In-situ and laboratory investigation on leaching and effects of early curing of shotcrete. *Nordic Concrete Research* 61, pp 23-37, 2019.

A. Sjölander, R. Hellgren, R. Malm and A. Ansell. Verification of failure mechanisms and design philosophy for a bolt-anchored and fibre-reinforced shotcrete lining. Accepted for publication in: *Engineering Failure Analysis*, 2020.

A. Sjölander, A. Ansell and R. Malm. Variations in rock support capacity due to local variations in bond strength and shotcrete thickness. Submitted to: *Tunnelling and Underground Space Technology*, February 2020.

A. Sjölander. *Structural behaviour of shotcrete in hard rock tunnels.* Doctoral thesis. KTH Royal Institute of Technology. Stockholm, Sweden, 2020.

Contents

Chapter 1

Introduction

In this chapter, the background to this report is presented first. Thereafter, the aims and goals, the limitations and the structure of this report are presented.

1.1 Background

Shotcrete is sprayed concrete applied pneumatically under high air pressure. The technique was initially developed by Carl Akeley at the Field Columbian Museum at the beginning of the 1900's [115]. To create realistic animal models for the museum, Akeley developed a small machine that used compressed air to spray gypsum. At this time the museum facades were in bad condition, and Akeley was asked to improve his machine to paint the facades with a layer of gypsum. Akeley and his colleague Clarence L. Dewey then developed the "plaster gun" that used compressed air to spray dry gypsum through a hose [115]. Akeley's invention was introduced as the "Cement Gun" in 1910 [123]. In the USA, the first attempts to use shotcrete as underground support were carried out in 1914 [19]. In Europe and Iran, shotcrete was used for the first time during the 1930's [10]. In 1955, a significant change in production method was introduced with the wet-mix method [80]. Until then, the dry-mix method had been used, where water was added to a dry shotcrete mix at the nozzle during spraying. This method produced much dust, which decreased with the wet-mix method [43]. According to Vandewalle [121], a lower rebound and higher spraying capacity can generally be achieved with the wet-mix method. Furthermore, compounded shotcrete could be delivered from the factories, which increased the control of the water-cement (w/c) ratio of the mix. Fibres were introduced in the shotcrete as reinforcement in the 1970s [43; 80]. Fibres are added to the shotcrete mix at the factory and remove the time-consuming work of placing steel bars as reinforcement. Since the 1980s, wet-sprayed fibre-reinforced shotcrete (FRS) has been the dominating support method for tunnels constructed in hard rock [43; 60; 85]. In the beginning of the 2000's, alkali-free set-accelerators were introduced. These reduced the negative effects with respect to strength development of the shotcrete and made it possible to spray thicker sections [69; 92]. In recent years, digital technology with

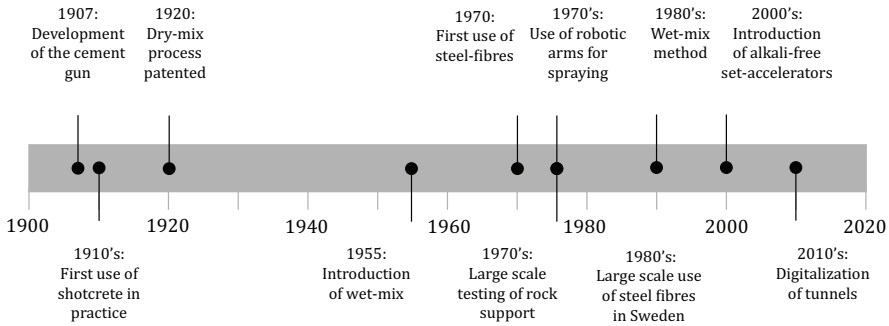

Figure 1.1: Time line for important achievements for shotcrete. From Franzén [43], Morgan [80], Nordström [85], Vandewalle [121] and Yoggi [123].

the use of e.g. LiDAR scanners to measure the shotcrete thickness have become more available and popular to use [41; 70]. This opens up for a better control of the actual sprayed thickness. During spraying, shotcrete sticks to the rock surface. This is achieved by applying shotcrete under high air pressure and using set accelerators, which makes the shotcrete stiffen rapidly. Therefore, no form-work is needed during construction, and with the use of FRS, a significant amount of time can be saved during construction. Due to the decreased production time and cost of labour, shotcrete is, when applicable, the obvious first choice for rock support. A time-line for important achievements in shotcrete history is shown in Figure 1.1.

Most tunnels in hard and jointed rock of good quality are excavated using the drill and blast method. Commonly, the roof of the tunnel is given an arch shape to enable the rock mass to support its self-weight. The stability of such a tunnel depends on the stability of the blocks in the arch [113]. High horizontal in-situ stresses in the rock mass could induce rotational forces on the block and push them out, while low horizontal stresses could cause blocks to loose contact and fall out. Therefore, tunnels are generally supported with FRS in combination with rock bolts. The main principle of this support system is that rock bolts are used to secure large and potentially loose blocks while FRS is used to support smaller blocks. Typically, a small block corresponds to a size that fits between a group of rock bolts. The structural behaviour of this support system is complex and involves the interaction between hard rock, FRS and rock bolts. Moreover, the loads acting on the support system are difficult to predict. Therefore, the design of rock support is commonly based on a classification system or simplified numerical calculations. Examples of classification systems are the Q-method developed by Barton et al. [11], and the rock mass rating system (RMR) developed by Bieniawski [15]. When designing the rock support with a classification system, the rock quality is evaluated based on a few parameters which gives a quality value for the rock mass, e.g. a Q or a RMR value. This, in combination with the tunnel geometry, results in a recommended rock support system. In Figure 1.2, the alternatives for rock support according to the Q-system [11] are shown. When using

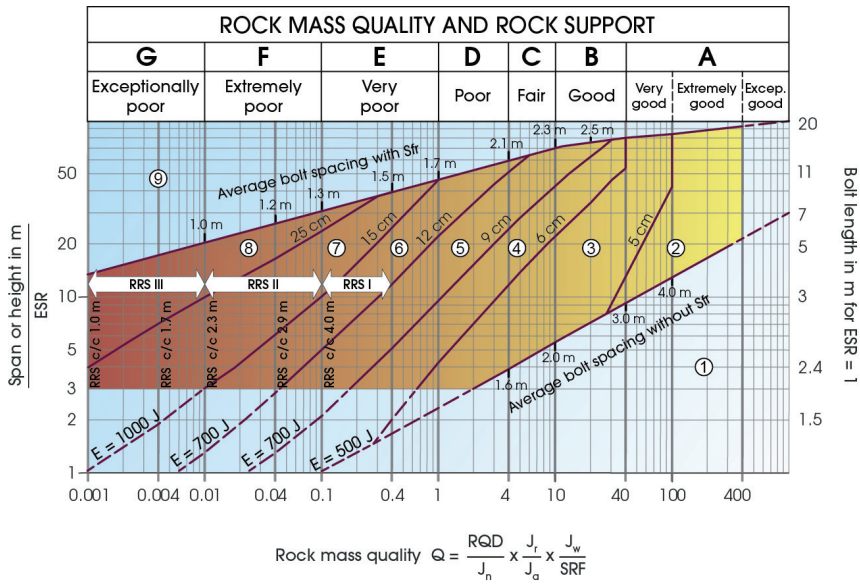

Figure 1.2: Recommended rock support based on the Q-method. From Barton et al. [11].

numerical or analytical solutions, the shotcrete is usually designed to support the load from a loose block, see e.g. Barrett and McCreath [10]. Here, the required shotcrete thickness, residual strength and bond strength are calculated based on individual failure modes.

Based on the literature review of failures in hard rock tunnels presented by Sjölander [100], it can be concluded that few major failures, i.e. cave-in failure in which pieces of rock or shotcrete falls down, are reported in the literature. Two cases with cave-ins are reported by Nilsen [84]. Both of them, the Oslofjord tunnel and the Hanekleiv tunnel, are located in Norway and the failures occurred in 2003 and 2006, respectively, while the tunnels were in operation. According to Nilsen [84] and Mao et al. [79], swelling clay was present in both cases, which was one of the driving forces for the failures. Obviously, the rock support was insufficient in both cases. However, the cause of failure is believed to be a result of that the rock mass quality and the consequences of the swelling clay was not estimated correctly. This means that classification systems will yield a safe design if the rock mass is classified correctly, but extra attention should be put to detect the presence of potential weak zones and swelling clays. Overall, based on the few reported failures in the literature, it can be concluded that the design approach used today generally results in a safe structure.

The downside of this design methodology is that the level of safety cannot be assessed. For numerical calculations, the in-situ variations in shotcrete thickness and bond strength to the rock are, normally, not considered. Data from the field

presented by Ansell [5] and by Malmgren et al. [78], indicate that the shotcrete thickness may vary significantly, with respect to the ordered thickness. Furthermore, the bond strength for shotcrete depends on factors such as; rock type, purity of the surface and the skill of the operator, see, e.g. Hahn [49], Malmgren et al. [78], Austin and Robins [6] and Thomas [116]. Therefore, local variations in bond strength are expected. Nevertheless, the design based on classification systems or analytical solutions yield a minimum shotcrete thickness and required bond strength, but how the in-situ variations in these parameters affect the structural behaviour of the shotcrete is today not fully understood. This leads to uncertainties that arise during construction in cases when the required thickness and bond strength are not fulfilled. Potentially, this may lead to that extra rock bolts or additional shotcrete are installed to secure the rock mass. This might be unnecessary and increase the cost for the tunnel and use of materials.

1.2 Aims and goals

The aim of this report is to describe and explain how the variations in shotcrete thickness and bond strength affect the structural behaviour and capacity for a shotcrete lining. For this purpose, a numerical framework has been developed. This framework consists of modelling strategies and material models for structural analysis of fibre-reinforced shotcrete, including interaction with hard rock and rock bolts. To be able to study the failure of a shotcrete support, the governing failure mechanism for shotcrete, the shotcrete-rock interface and rock bolts have been included. Especially, this report aims at answering the following research questions:

1. How can the in-situ distribution of shotcrete thickness and bond strength be described?
2. How will a local area without bond affect the cracking of a shotcrete lining subjected to shrinkage?
3. How does the varying thickness of the shotcrete lining affect its cracking when it is subjected to drying shrinkage?
4. Is the failure of a shotcrete lining governed by local areas with low shotcrete thickness or bond strength?
5. Is it suitable to design a shotcrete lining for individual failure modes or should a combination be considered?

1.3 Limitations

This report is limited to the study of large scale use of wet-sprayed shotcrete to support hard and jointed rock. The work presented within this report is based on numerical simulations considering quasi-static load conditions with no effect due to time-dependent deformations, i.e. no consideration was taken to dynamic effects or deformation due to creep. For studies regarding dynamically loaded shotcrete, see e.g. Holmgren [57; 59], Ansell [4] and Ahmed [2]. The focus in this report was the structural behaviour of the shotcrete and its interaction with the rock and rock bolts. Relevant material data to describe the elastic and non-linear behaviour of shotcrete, rock and rock bolts were based on experimental data from the literature.

1.4 Structure of the report

Chapter 2 gives a background to the construction and the design of tunnels in hard rock. This includes an overview of different support methods used for hard rock tunnels, design methods and fibre-reinforced shotcrete. In Chapter 3, the numerical model used in this report is presented. The results from the studied cases are presented in Chapter 4, which is followed by a general discussion of the results in Chapter 5. Finally, the conclusions and suggestions for further research are presented in Chapter 6.

Chapter 2

Support of hard rock tunnels

In this chapter, an overview of different support systems for tunnels in hard rock is presented. This is followed by a presentation of the design principles for rock support. The chapter is concluded with a general presentation of fibre-reinforced shotcrete and bond strength.

2.1 Overview of different types of support

According to Hoek and Brown [53], the main principle in the design of rock tunnels is to enable the rock mass to support its weight. Before an excavation takes place, the rock mass is in equilibrium with an initial state of stress. This will, due to the excavation, be locally disrupted [54]. Basically, this means that the blocks around the tunnel perimeter will lose the potential support that was provided by the excavated rock mass. For blocks in the tunnel roof, the weight from the rock mass must, therefore, be transferred to the surrounding rock mass, either by tension or by compression. In a jointed rock mass, no tensile stress can be transferred along the joints. Normally, such tunnels are excavated in an arch shape, and the stability of the tunnel depends, to a great extent, on the interlocking between individual blocks [113]. Falling blocks is one of the most common failure modes in a tunnel [55]. This is caused by a loss of contact between blocks due to low horizontal stresses, or to exceeded friction forces along the rock joints [113].

Rock bolts and fibre-reinforced shotcrete (FRS) are commonly used in hard rock tunnels to support the rock mass. In some cases, only one of the components is used, but more often rock bolts are used in combination with FRS. Rock bolts can be placed to secure individual blocks, by spot bolting, or systematically. Grouted rock bolts are often used to ensure the structural connection between the rock bolt and rock mass, while the load between the shotcrete and the rock bolts is transferred through steel washer plates. Thus, the deformation of the rock mass results in tensile forces in the bolt, and a compressive force between the washer plate and

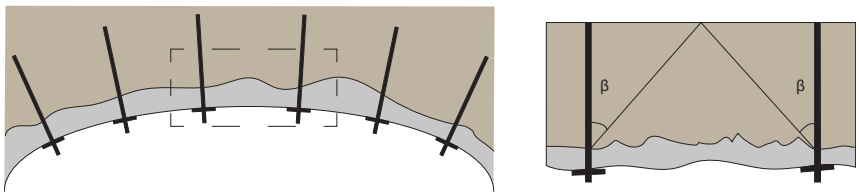

Figure 2.1: Load model to estimate the volume of a loose block between bolts. Redrawn from Barrett and McCreath [10].

the shotcrete. The compressive forces from the washer plates will be distributed through the rock mass and for systematically placed bolts, a zone in complete compression exists at a certain distance from the plate. This concept is shown in Figure 2.1 and ensures that a compressive zone develops in the arch. This also illustrates that between the washer plates, zones with potentially loose blocks exist which must be supported by shotcrete. Blocks are supported by shotcrete either through the bond strength between shotcrete and rock or the mechanical strength of the shotcrete. Furthermore, it is believed that shotcrete, which is applied under high air pressure, will penetrate and partly fill up rock joints [111]. Thus, a contact surface is generated, which enables that a contact pressure can develop between the blocks [19; 113]. The load from a block can also be transferred to the surrounding rock mass or rock bolts through the bond between shotcrete and rock, or the flexural capacity of the shotcrete. Additionally, shotcrete seals the rock surface, which reduces the risk for rock joints drying. For exposed rock joints, there is a risk that the material from the joints is transported away, which could lead to lost contact between two blocks.

For road tunnels, infiltrating water could form ice on the road surface, which reduces the safety with respect to traffic. Moreover, water is a common source for deterioration of the shotcrete [62; 103]. Therefore, water must be removed from the tunnel environment, and different methods and techniques exist. Normally, pre-grouting is performed in which a cement mix is pumped into the rock mass through drilled holes. The fine grained cement mix should be able to distribute and fill up existing rock joints, and thereby seal the rock mass. The result from pre-grouting is not always satisfactory, and in those situations is a drainage system installed in combination with the shotcrete. One example of such a system, which was used in the construction of the Southern Link motorway tunnel in Stockholm, Sweden (opened 2004), is shown in top of Figure 2.2. Here, sections with infiltrating water were covered with a synthetic drain mat and a drainage pipe to create a dry environment for the traffic [44]. The drain mats were fixed to the rock with bolts and then covered with a layer of FRS. At the end of each section, the rock was exposed to enable bonding between shotcrete and rock, and thus creating an end-restrained structural system. Before the tunnel was opened for traffic, a large number of shrinkage cracks were found in the shotcrete [60]. The reason for the cracking was the drying shrinkage of the shotcrete, as presented by Ansell [5].

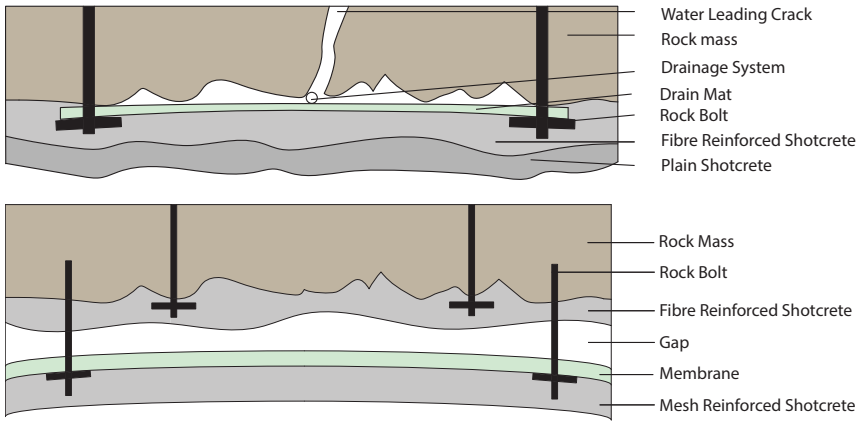

Figure 2.2: Different rock support systems used in Sweden for sections with infiltrating water. System with synthetic drain-mats (top) and inner lining system (bottom).

Due to this problem, a system with an inner lining has been used in two recently constructed motorway and railway tunnels in Sweden, see the bottom of Figure 2.2. According to [86], this system should streamline the construction phase and result in a dry traffic environment in the tunnel. This system is built-up of two separate shotcrete linings; one for structural support and one to create a dry traffic environment. The first lining is the primary rock support, and consists of rock bolts in combination with FRS sprayed directly on the rock surface. Then, for the second lining, a waterproof membrane is applied to cover the roof and walls of the tunnel. Additional rock bolts are placed to keep the membrane in place and a layer of mesh reinforcement is placed before shotcrete is sprayed. This creates a free-standing arch in which FRS is combined with mesh reinforcement. One downside with this system is that the primary rock support is covered and not easy to inspect.

The principle described above, with two separate linings, has traditionally been used in Norwegian tunnels. However, according to Holter [61], a new composite lining system is being considered to replace this system. The idea is to use rock bolts and FRS sprayed directly against the rock. Then, a thin (2-4 mm) water-proof membrane is sprayed on the shotcrete. The membrane bonds to the shotcrete and a second layer of FRS is then sprayed to cover the membrane. This support system is shown in the top of Figure 2.3. The moisture transportation and mechanical properties of this composite lining are presented by Holter [62; 63; 64]. Outside of the Nordic countries, there is some ongoing research on supporting the rock with thin polymer linings, see the bottom of Figure 2.3. These linings are fast setting and have a thickness of around 2-5 mm [89]. An obvious advantage with such a thin lining is the reduced application time and transportation of material. Tannant [114] discuss some structural principles of thin liners, while Ozturk and Tannant [91; 90] present experimental results for the adhesion between the lining and the rock surface.

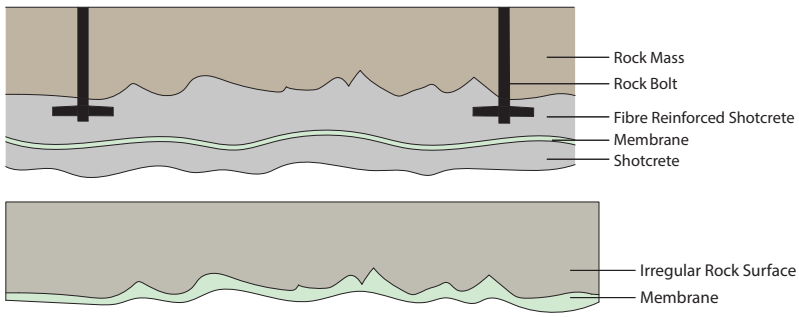

Figure 2.3: Top figure shows a composite FRS lining with a thin water-proof membrane, from Holter [61]. Bottom figure shows the principle of a thin sprayed polymer lining, from Ozturk [89].

2.2 Design of rock support in hard rock

The design of civil engineering structures within most parts of Europe must follow Eurocode [27]. For the design of geotechnical structures, Eurocode 7 (EC7)[29] applies. In contrast to the design of structures built with concrete, timber or steel, the design of geotechnical structures must not necessarily be verified by numerical calculations. According to EC7, the limit states for a structure should be verified by any, or a combination, of the following methods:

- Adoption of prescriptive measures.
- Experimental models and tests.
- The observational method.
- Design calculations.

The reason for this approach is the many uncertainties related to the design. For tunnels, large uncertainties normally exist regarding the rock mass quality, orientation of joints and water conditions, which makes it difficult to state the mechanical properties of the rock with a high degree of certainty. Therefore, predicting the structural behaviour of the tunnel after excavation, i.e. the deformation of the rock mass, is not an easy task. Furthermore, it is difficult to predict the loads that act on the rock support system. According to Holter [61], only a few cases with detailed monitoring of loads acting on the rock support are presented in the literature.

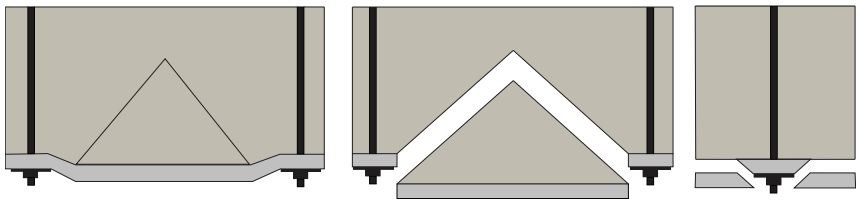

Figure 2.4: Failure modes for a shotcrete lining subjected to a block load. From left to right, flexural, direct shear, and punching shear failure. Redrawn from Bjureland et al. [16].

The adoption of prescriptive measures means that the tunnel could be designed solely based on empirical methods. This type of design is based on a rock mass classification system such as; the Q-method, developed by Barton et al. [11], or the rock mass rating system (RMR), developed by Bieniawski [15]. Both systems are based on an estimation of the rock mass quality by determination of a few fixed parameters such as; the strength of intact rock, characteristics and number of joints and water conditions. This yield an RMR value between 0 and 100, or a Q-value from 0 to 1000, which together with the excavation shape and geometry yields a recommended rock support. According to Palmström and Stille [113], a design solely based on rock mass classification system should be sufficient for minor tunnels in good quality rock. However, for a more complex project, the combination of a classification system, numerical analyses and the observational method should be used to ensure a safe design [113].

For the design of shotcrete using numerical methods, the gravity load from a loose block that fits between a group of rock bolts is commonly used. Different failure modes for this load is presented by e.g. Barrett and McCreath [10]. Which failure mode that develops depend primarily on the bond strength. If the block can be carried through the bond, a direct shear failure can occur. If the bond fails, flexural failure of the shotcrete or punching shear failure at the rock bolts could occur. These failure modes are illustrated in Figure 2.4, and were used to define the mechanical system for the probabilistic verification of the rock support capacity in [16].

Most of the theoretical knowledge regarding the failure of a bolt-anchored and fibre-reinforced shotcrete lining is derived from full-scale experimental testing presented by Fernandes-Delgado et al. [42] and by Holmgren [56; 58]. Based on the results by Holmgren [56], Stille [112] suggested a linear relationship between the width of the load transfer band δ_{b} and the shotcrete thickness. This has been implemented in the design guidelines for Swedish rock tunnels [118], where it is suggested that δ_{b} increases linearly between 25 and 35 mm for a shotcrete thickness in the range between 40 and 80 mm. However, it should be stressed that the suggested linear relationship by Stille [112] was based on few samples with differences in curing time. The relationship between δ_{b} and the shotcrete thickness is therefore considered to be uncertain. The load capacity for a shotcrete lining, with

respect to bond failure, and how it is affected by local variations in bond strength and shotcrete thickness was investigated by Sjölander et al. [106]. The failure mechanisms for a bolt-anchored and fibre-reinforced shotcrete lining was investigated by Sjölander et al. [105]. The results from these studies are presented and discussed in Section 4.3.

2.3 Fibre reinforced shotcrete

Shotcrete is sprayed concrete that is applied pneumatically under high pressure to a surface. Upon hitting the surface, the large momentum compacts the shotcrete directly, and vibration of the shotcrete is therefore not necessary. Today, alkali-free set accelerators are often used and mixed into the shotcrete at the nozzle [94]. In contact with cement and water, the set accelerator will react and build up an ettringite structure. This makes the shotcrete stiff enough to stick to the surface. Compared to non alkali free set accelerators, the benefits of alkali-free accelerators are; a higher final strength of the shotcrete and an earlier onset of the silicate reactions in the cement which promotes the strength development of the shotcrete [94]. The cement content is normally around 400 kg/m^3, or more [20; 83], to increase the workability and pumpability of the shotcrete. Large aggregates tend to rebound to a larger extent from the surface than smaller ones, and the maximum aggregate size is therefore often restricted to 8 mm. This makes the shotcrete easier to pump and prevents aggregates from getting stuck in the hose.

Compared to cast concrete, the use of set accelerators, high cement content, and high volume fraction of fines in the shotcrete will affect the development of the material strength. Furthermore, the amount of shrinkage and the structural effects due to creep do not necessarily follow that of ordinary concrete. Lately, this has gained increased interest from the scientific community and studies regarding the development of material strength is presented by e.g. Bryne [20] and Hammer et al. [50]. The creep behaviour has been experimentally investigated by Neuner et al. [83], while the magnitude and structural effects of shrinkage for continuously and end-restrained shotcrete specimens have been studied by Lagerblad et al. [69], Leung et al. [71] and Malmgren et al. [78].

During the spraying process, it is difficult to determine the applied thickness. This is due to the fact that the visibility during spraying is limited, the material will rebound from the surface, and there is no natural reference to determine the thickness. Furthermore, a tunnel excavated with the drill-and-blast method will have an irregular surface, which makes it more difficult to determine the thickness. Therefore, local variations in shotcrete thickness are expected. In-situ investigations by Malmgren et al. [78] and Ansell [5] have shown that the required thickness often is achieved, see Table 2.1 and Figure 2.5.

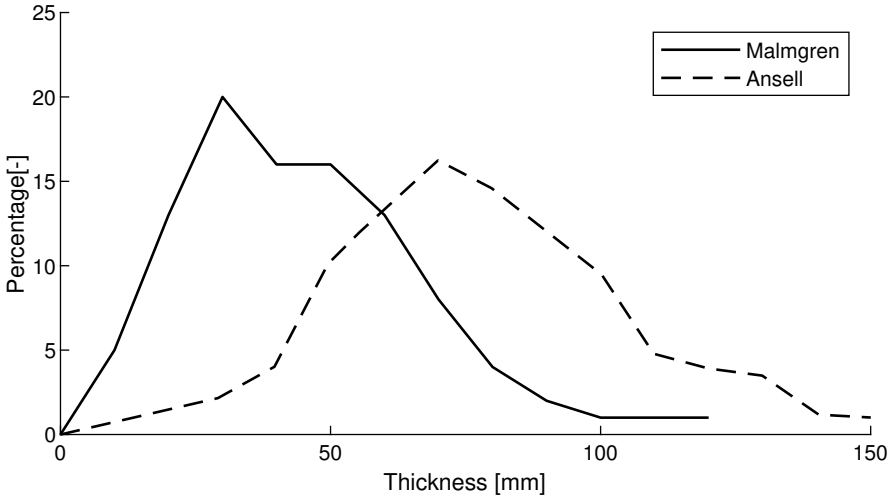

Figure 2.5: Distribution of shotcrete thickness. Reproduced from Malmgren et al. [78] and Ansell [5].

Table 2.1: In situ measurement of thickness of applied shotcrete

Reference	**Thickness [mm]**		
	Required	**Mean**	**St.D**
Södra Länken [5]	60	72	27
LKAB [78]	30-50	42	23

Today, technical solutions exist that could reduce the unnecessary use of shotcrete. Wetlesen and Krutrök [122] present result from a case study performed in the LKAB mines, in which a laser scanner system was mounted on the spray robot. When using this system, the rock surface was first scanned. Then shotcrete was sprayed, and its surface was scanned. The system could then provide the operator with a topographic map, highlighting sections with insufficient shotcrete thickness. According to Wetlesen and Krutrök [122], the accuracy of the system is within 5 mm and the use of shotcrete was reduced with more than 20% when the laser scanner system was used.

Unreinforced shotcrete has a quasi-brittle failure in tension and must be reinforced to increase its ductility. The reinforcement consists typically of fibres or steel-bars. Steel fibres were first introduced as reinforcement during the 1970's [43; 80] and have since then been the predominant reinforcement used for tunnel applications. The reason for this is simply because the use of fibres reduces the time-consuming work of placing steel bars against the uneven rock surface.

There are two different main categories of fibres; micro and macro. Microfibres are generally defined as fibres with a diameter of less than 0.3 mm. Microfibres have no effects on the ductility of the shotcrete and are added to enhance other properties. For instance, polypropylene (PP) fibres are typically added to decrease the risk of fire spalling of the shotcrete [67]. Microfibres are also used to reduce plastic shrinkage cracking. Macro fibres have a diameter larger than 0.3 mm, and are added to increase the ductility of the shotcrete. Today, macro fibres are mainly produced by steel, basalt or synthetic materials. The fibres exist in many different shapes, and some examples of steel, synthetic and basalt fibre types are shown in Figure 2.6. In Sweden, there is a strong tradition of using steel fibres, and in road and railway tunnels no other type of fibres are allowed today. In Norway, there is a similar situation, and macro polypropylene fibres are prohibited from use in road tunnels since November 2015 [81]. Therefore, the structural behaviour of steel fibre-reinforced shotcrete has been the focus of this report.

Two things are important to consider when adding fibres to shotcrete; fibres must be able to pass through the hose and nozzle during spraying, and fibres must be able to disperse evenly in the shotcrete mix. Depending on project regulations, the shotcrete should either fulfil demands for energy absorption or a residual strength. Usually, 40 to 60 kg/m^3 of steel fibres with one set of end-hooks and a

Figure 2.6: Different type of macro (structural) fibres. From left to right, steel fibres with various end-hooks (1-3), synthetic fibres (4-5) and basalt fibres (6-7).

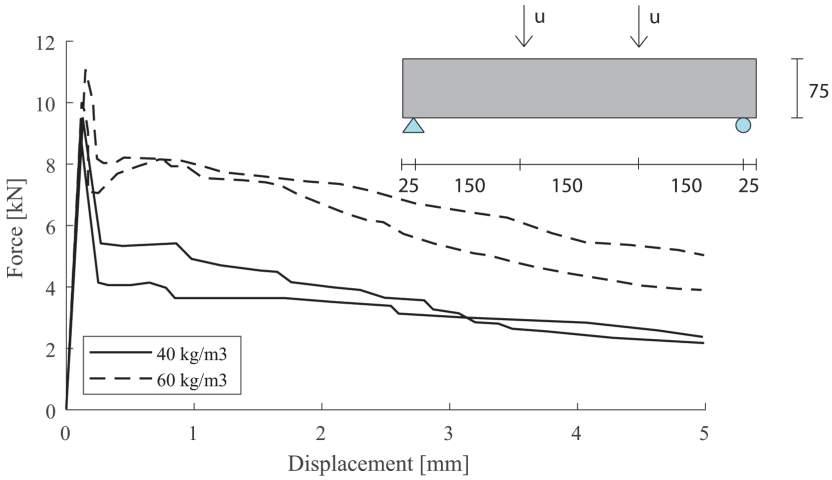

Figure 2.7: Relationship between force and vertical displacement for fibre reinforced shotcrete subjected to four-point bending according to EN-14488-3 [30]. Results from El Zain [40].

length of 30 to 40 mm are added to the shotcrete used as rock support in Sweden [5; 20; 78]. This will result in a strain-softening behaviour, and some example on the relationship between force and vertical displacement for a standard four-point bending test according to EN-14488-3 [30], and presented by El-Zain [40], are here shown in Figure 2.7. In these tests, 40 and 60 kg/m^3 of end-hooked fibres of the type CHO-65/35 from Sika were used. Before cracking, the effect from the fibres is negligible. The response up to the peak load is, therefore, governed by the elastic stiffness and tensile strength of the shotcrete. After cracking, a characteristic reduction in force can be seen. This is due to that the fibres bridging the crack are unable to absorb the released elastic energy caused by cracking. Therefore, the reduction of the force depends on the amount and efficiency of the fibres bridging the crack. As seen in Figure 2.7, the reduction in force decreases with an increased amount of fibres. The primary energy consumption mechanism after cracking is sliding of the fibres along the shotcrete matrix [8]. Therefore, the efficiency of the fibres depends on the bond properties between fibre and shotcrete, as well as on the shape of the fibre and design of end-hooks. Moreover, the orientation of the fibres with respect to the crack also affects the post-cracking behaviour. The structural response shown in Figure 2.7 indicates a strain-softening behaviour in which, normally, only one crack forms during experimental failure tests.

For numerical simulations of FRS, two main approaches exist; implicit and explicit modelling. In the latter, fibres are modelled as individual parts. Such models are complex, and must be derived based on the pull-out behaviour of individual fibres. To achieve a realistic response, the variation in pull-out behaviour due to the embedment length and orientation of the fibre with respect to the force must also be accounted for. The inclination of the fibres to the force must be included to

achieve realistic results. Moreover, the fibres must be distributed within the model in a representative way. An interesting approach for such a model is presented by Soetens and Matthys [108], who used a Monte-Carlo sampling algorithm to distribute the fibres randomly within a specimen. This type of models is computational heavy and more suitable for the study on failure mechanisms of fibres during cracking, i.e. if fibres fail due to pull-out or tensile stress. The structural analyses performed in this report were based on an implicit model. In such, individual fibres are not modelled, and instead the effect of the fibres are smeared over the shotcrete mass. Basically, this means that the fracture energy of the shotcrete is increased to account for the increased ductility. Such a model is more suitable for analyses when the structural behaviour is to be studied.

2.4 Bond strength between shotcrete and rock

The bond strength between shotcrete and rock is a decisive parameter for the structural behaviour of a shotcrete lining. Furthermore, a high early bond strength is essential to achieve a safe and efficient rock support. It was shown by Bryne et al. [21] that the development of bond strength between accelerated shotcrete and granite is fast, and values up to 1.0 MPa can be reached within 24 hours. With a continuous bond between the two materials, composite action is achieved which greatly affects the structural behaviour for the shotcrete. Laboratory tests presented by Carlswärd [26] and numerical simulations presented by A. Sjölander and A. Ansell [101] showed that a pattern of fine and narrow cracks form in unreinforced shotcrete subjected to shrinkage when a continuous bond exist. Furthermore, experimental testing by Fernandez-Delgado et al. [42] and by Holmgren [56; 58] has shown that the interface can carry a substantial load. In Figure 2.8, some results from Holmgren [58] are shown to illustrate the load capacity for a bonded shotcrete lining. How variations on shotcrete thickness and bond strength affect the structural capacity, with respect to bond failure, was investigated by Sjölander et al. [106].

The bond strength between concrete and different types of aggregates is well studied, with many papers devoted to experimental testing, see e.g. Tschegg et al. [119; 120] and Alexander et al. [3]. How the mineral composition and the surface roughness of the rock affect the bond strength was presented by Hahn [49]. Through extensive testing, it was concluded that the mineral composition, i.e. the rock type, is the more important factor for the bond strength [49]. Some results from this study are presented in Table 2.2, and it can be noted that the significance of surface roughness seems to vary for different rock types. The bond strength between two surfaces depends to a great extent on the quality and cleanliness of the contact faces [7; 97]. The importance of the rock surface condition, with respect to failure mode and bond strength, was shown in a study by Malmgren et al. [76]. In this, the rock surface was treated with either; *i*) mechanical

Table 2.2: Compilation of bond strength between shotcrete and various rock types and surface roughness. From Hahn [49].

Rocktype	Grain size	Bond strength [MPa]	
		Smooth surface	Rough Surface
Shale	Very fine grained	0.24	0.28
Lime stone-marlstone	Middle grained	1.49	1.89
Marble	Fine grained	1.38	1.52
Granite	Middle grained	1.04	1.40
Granite	Fine-Middle grained	1.48	1.71

scaling followed by cleaning with a water pressure of 0.7 MPa or *ii*), hydro-scaling with a pressure of 22 MPa. The difference was clear, in *i*) the mean value of the bond strength was 0.18 MPa, and 65% of the failures occurred in the rock mass. For *ii*), the mean value of the bond strength was 0.59 MPa, and 58% of the failures occurred along the interface between shotcrete and rock. Thus, hydro-scaling removes low-quality rock, which reduces the number of failures that occurs in the rock mass. This removes many of the failures that occur for a low bond strength, which increases the mean bond strength. How the surface preparation affects the bond strength for a concrete-to-concrete interface was studied by Austin et al. [7] and by Silfwerbrand [95]. From these studies, it was concluded that the bond strength increased for a surface treated with hydro-scaling, compared to a pneumatic hammer. The reason for this is likely that the pneumatic hammer will cause more microcracks on the surface. According to Austin et al. [7], microcracks at the contact surface will introduce stress concentrations which could effect the tensile bond strength.

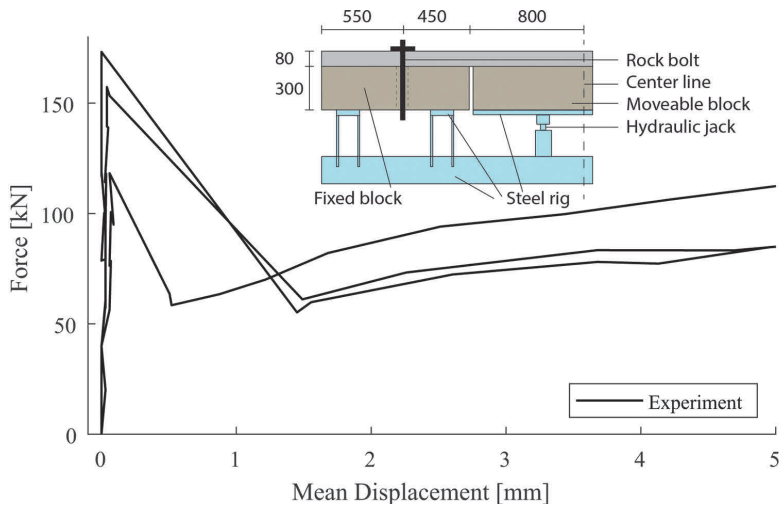

Figure 2.8: Examples of structural capacity for a bonded shotcrete lining subjected to the load from a loose block and the experimental set-up, in which a hydraulic jack was used to push the centre block through the shotcrete. Reproduced from Holmgren [58].

Chapter 3

Numerical modelling of shotcrete

In this chapter, the numerical models used in this report are described. All material models are based on damage mechanics and some basic concepts valid for all models are therefore summarized first. Then, the models for unreinforced and fibre-reinforced shotcrete (FRS) is presented. This is followed by the model used to describe the interface failure between shotcrete and rock. After that, the numerical model to simulate pull-out failure of rock bolts and a multi-physical approach of modelling drying shrinkage is presented.

3.1 Damage mechanics

Non-linear behaviour of materials is commonly described with fracture mechanics, damage mechanics or theory of plasticity. In the work by A. Sjölander and A. Ansell [101], the concrete damaged plasticity model (CDP) implemented in the finite element (FE) software Abaqus [1] was used to describe the non-linear behaviour of glass fibre-reinforced shotcrete. For the majority of the work with this report, the post-cracking behaviour of shotcrete was described using damage mechanics, and this concept is therefore presented below. In general, a model based on damage mechanics is more computationally efficient compared to a plasticity model [88; 98; 99], which was the main reason for using this type of model in [102; 105; 106].

The pioneering work within damage mechanics is commonly acknowledged to Kachanov [68]. In damage mechanics, the effect of fracture of a material is described with a decreased load-bearing area, which results in a reduced stiffness of the material. This is illustrated in Figure 3.1, in which the left side schematically shows the softening response for an unreinforced shotcrete specimen shown to the right in the figure.

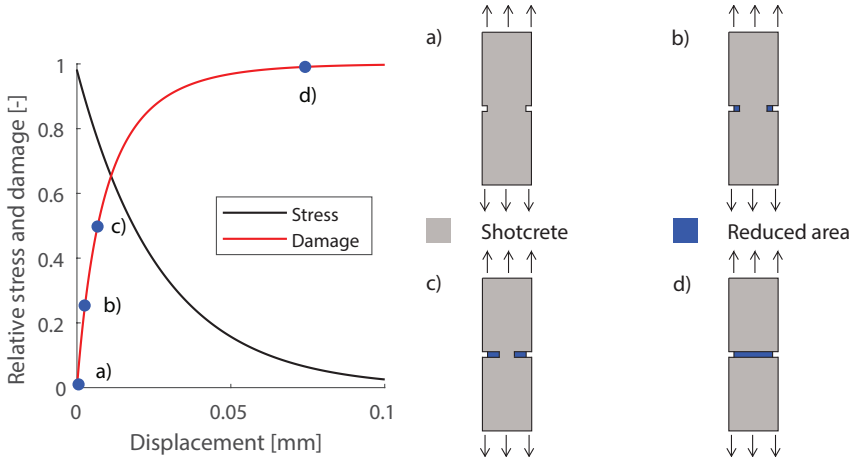

Figure 3.1: Illustration of the concept of damage mechanics. Left figure shows the relationship between normalized stress and evolution of damage in one element during cracking of an unreinforced shotcrete specimen. The right figure illustrates the original load bearing area (a) and its reduction at three different damage levels , b-d.

In this report, materials have initially been considered free from damage and a linear relationship between stress and displacement has been assumed up to the point of failure initiation. After that point, the cohesive crack model, as presented by Hillerborg et al. [52], was used. In this model, a fracture process zone (FPZ) exist in front of the crack tip, and the stress σ is described as a function of the crack opening w, until a stress-free crack opening w_{f} is reached. Commonly, the shape of the $\sigma(w)$-function, e.g. bi-linear, tri-linear or exponential, is determined based on observation of results from experimental testing, e.g. the relationship between force and vertical displacement from four-point bending tests. Then, input data for the selected $\sigma(w)$-function are decided based on fitting simulated results to experimental data. The cohesive crack model is illustrated with the stress distribution along the shotcrete-rock interface in Figure 3.2. During separation, the tensile bond stresses are distributed over a certain length, here denoted δ_{b}. At the crack tip, the tensile bond strength σ_{If} is reached and a linear elastic stress distribution exists in front of the crack tip. As can be seen in Figure 3.2, an exponential softening function was used to describe the stress distribution behind the crack tip.

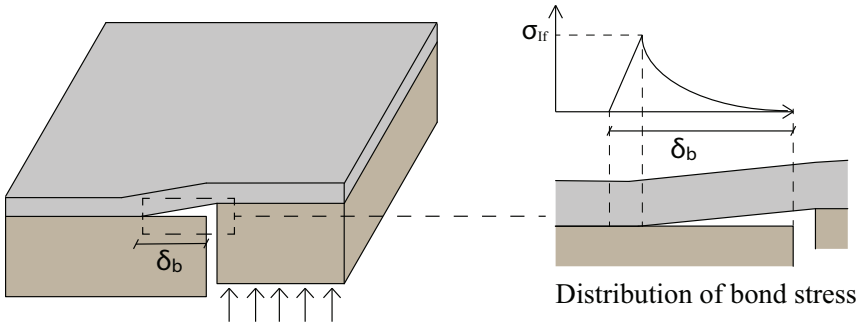

Figure 3.2: Example of stress distribution along the interface between shotcrete and rock during separation with the cohesive crack model. Redrawn from Sjölander et al. [106].

3.2 Modelling of shotcrete

Below, the governing equations for unreinforced shotcrete are presented. Then, the additional equations needed to consider fibres are given. The numerical framework for the model is based on the work by Oliver et al. [88], and the implementation of the governing equations in the FE software Comsol Multiphysics [35] is based on the work by Gasch [45; 46].

The damage model is based on pure Mode-I failure, i.e. tensile cracking of shotcrete, and the progression of damage was described with an isotropic damage model. Initially, there is a linear relationship between stress σ and strain ε, following Hooke's law. When the tensile strength σ_{t} is reached, cracking occurs and damage initiates. The evolution of damage is described by ω, which ranges from zero for the undamaged material to one for a fully damaged material. The stress in the shotcrete is described by:

$$\sigma \;=\; (1-\omega)E\varepsilon_{\mathrm{eq}} \tag{3.1}$$

Here, E is the Young's modulus of the undamaged material and $\varepsilon_{\mathrm{eq}}$ the equivalent strain based on Rankine's theory, see Eq. (3.2). The interpretation of $\max\langle\sigma_{\mathrm{i}}\rangle$ is that only tensile stress was considered in the damage model.

$$\varepsilon_{\mathrm{eq}} \;=\; \frac{1}{E}\max\langle\sigma_{\mathrm{i}}\rangle, i = 1,2,3 \tag{3.2}$$

After cracking, the cohesive crack model was used to describe the relationship between stress σ and crack width w. The crack width should be implemented in a FE-software in terms of strains to decrease mesh dependency. For this purpose, the crack band width theory was used, see e.g. Bazant [13]. According to this the effect of microcracking that occurs in the FPZ is smeared over a crack band width. In the local damage model used here, the width of the band is defined equal to the mesh size h. The relation between crack width w and strain ε is expressed according to:

$$w \;=\; h\varepsilon_{\mathrm{i}} \tag{3.3}$$

The numerical interpretation of the crack band theory is that the reduction of stiffness, which is followed by cracking, is governed and restricted by the element size. Moreover, the release of fracture energy G_{f} is regulated by the element size. For non-linear FE analysis of concrete structures, a general recommendation [51; 75] is that the maximum element h_{cr} size should be less than:

$$h_{\mathrm{cr}} \;<\; \frac{EG_{\mathrm{f}}}{\sigma_{\mathrm{t}}} \tag{3.4}$$

Damage is irreversible and should, therefore, be evaluated based on the maximum history-dependent strain in each element. To ensure this, a history-dependent variable κ was defined according to Eq. (3.5). At each time-step, κ is defined as the maximum strain in the current time-step $\varepsilon_{\mathrm{eq}}$, and the previous maximum strain κ_{old}. Together with the conditions stated in Eqs. (3.6-3.7), damage ω can only increase when the current state of strain $\varepsilon_{\mathrm{eq}}$ is larger than the history-dependent strains κ.

$$\kappa \;=\; \max(\varepsilon_{\mathrm{eq}}, \kappa_{\mathrm{old}}) \tag{3.5}$$

$$f(\varepsilon_{\mathrm{eq}}, \kappa) \;=\; \varepsilon_{\mathrm{eq}} - \kappa \leq 0 \tag{3.6}$$

$$f \leq 0,\; \kappa' \geq 0,\; \kappa' f \;=\; 0 \tag{3.7}$$

From here on, the relationship between stress and crack width $\sigma(w)$ is instead described with the relationship between stress and strain $\sigma(\kappa)$. The softening behaviour of unreinforced shotcrete is commonly described with a bi-linear or an exponential function, see e.g. [47; 74; 88; 108]. Here, the latter was used.

$$\sigma(\kappa) \;=\; \sigma_{\mathrm{t}} \exp\left(\frac{\varepsilon_0 - \kappa}{\varepsilon_{\mathrm{f}}}\right) \text{ for } \kappa > \varepsilon_0 \tag{3.8}$$

In Eq. (3.8), $\varepsilon_0 = \sigma_{\mathrm{t}}/E$ is the strain at cracking and ε_{f} defines the shape of the softening curve as:

$$\varepsilon_{\mathrm{f}} \;=\; \frac{\varepsilon_0}{2} + \frac{G_{\mathrm{f}}}{\sigma_{\mathrm{t}}} \tag{3.9}$$

The damage function $\omega(\kappa)$ is derived by setting Eqs. (3.1) and (3.8) equal, which yields:

$$\omega(\kappa) \;=\; 1 - \frac{\varepsilon_0}{\kappa} \exp\left(\frac{\varepsilon_0 - \kappa}{\varepsilon_{\mathrm{f}}}\right) \text{ for } \kappa > \varepsilon_0 \tag{3.10}$$

The numerical model for fibre-reinforced shotcrete is based on the same governing equations as presented above. However, due to the increased ductility introduced by the fibres, a different $\sigma(\kappa)$-function was used. Numerically, this means that the increased ductility of the shotcrete was modelled by increasing the fracture energy. More specifically, the effect of the fibres was treated in an average sense, in which individual fibres were not modelled.

In this report, FRS was modelled with a combination of an exponential softening function and a bi-linear curve. This model was first presented by Sjölander et

al. [104]. The basic idea with this model is that the response from the shotcrete and fibres is separated. Therefore, the initial post-cracking response is governed by the fracture energy of unreinforced shotcrete. This is described with an exponential softening curve, as in Eq. (3.8). At a certain strain ε_{i}, i.e. crack width w_{i}, the fibres are activated. From this point, the relationship between stress and strain is described with a bi-linear curve. In Figure 3.3, the relationship between stress and strain for the fibre-reinforced shotcrete model is shown schematically.

The bi-linear function can account for hardening, perfect plasticity or softening, and was implemented as two linear functions. In Eq. (3.11), σ_{fi} is the stress when the strain is zero for each linear function.

$$\sigma_i(\kappa) \;=\; \sigma_{\mathrm{fi}} - k_{\mathrm{i}}\kappa \text{ for } \varepsilon_{\mathrm{i}-1} \leq \kappa < \varepsilon_{\mathrm{i}} \tag{3.11}$$

In this way, the linear variation in stress as a function of the strain κ can be expressed as the derivative of the linear function k_{i}, see Eq. (3.12), multiplied with the history-dependent maximum strain κ as defined in Eq. (3.5).

$$k_i \;=\; \frac{\Delta\sigma}{\Delta\kappa} \tag{3.12}$$

The damage function for each linear curve, $\omega_{\mathrm{i}}(\kappa)$ was derived by setting Eqs. (3.1) and (3.11) equal, which yields:

$$\omega_{\mathrm{i}}(\kappa) \;=\; 1 - \frac{\sigma_{\mathrm{fi}} - k_{\mathrm{i}}\kappa}{E\kappa} \text{ for } \varepsilon_{\mathrm{i}-1} < \kappa < \varepsilon_{\mathrm{i}} \tag{3.13}$$

In Figure 3.4, results from Sjölander et al. [104] are reproduced to show the capability of the FRS model. In [104], experimental results from notched and fibre-reinforced concrete beams subjected to three-point bending presented by Buratti

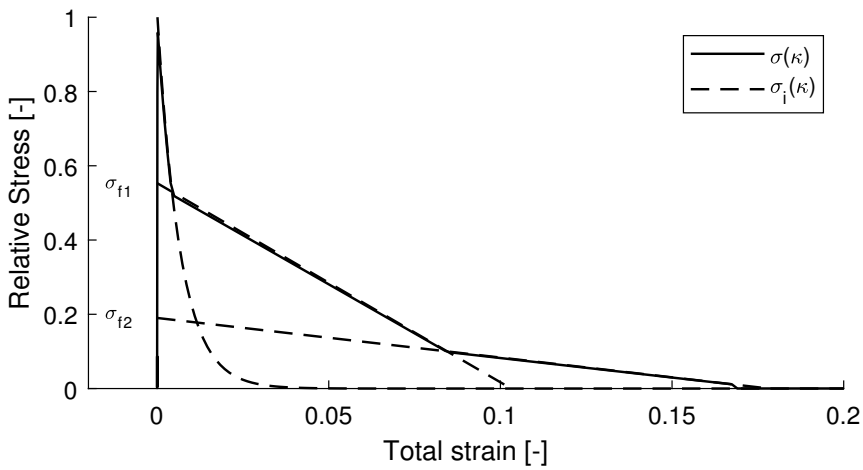

Figure 3.3: A schematic presentation of the relationship between relative stress and strain for the FRS model.

Table 3.1: Mechanical properties used in the numerical simulations. From Sjölander et al. [104].

σ_t **[MPa]**	G_f **[N/m]**	w_1 **[mm]**	w_2 **[mm]**	w_3 **[mm]**	α_2 **[-]**	α_3 **[-]**
3.2	100	0.045-0.065	1.75-2.50	5.0	0.18-0.30	0.01

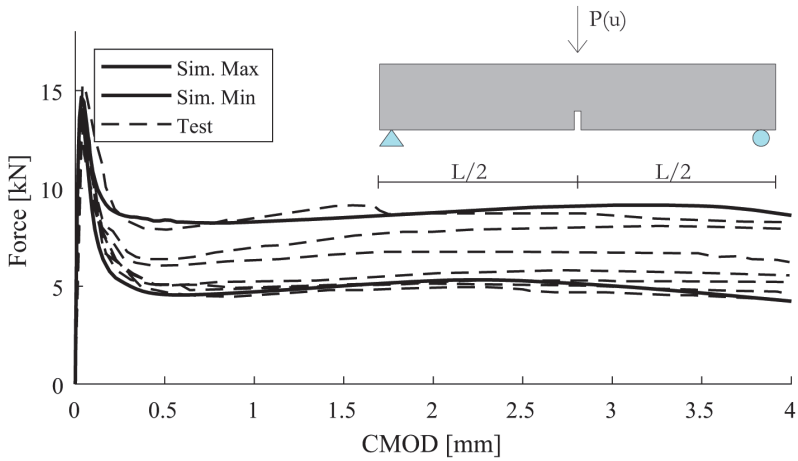

Figure 3.4: Comparison between numerical simulations and experimental results from Buratti et al. [24] and set-up for experiment. Reproduced from Sjölander et al. [104].

et al. [24] were used. A 2D numerical model with one fixed and one roller support was used for the simulation. A controlled displacement was applied, and the force and crack mouth opening displacement (CMOD) were plotted and compared to the experiments. The CMOD was in the simulations measured at the bottom of the notch. The mechanical properties for the models are presented in Table 3.1. Here, w_i and α_i are the crack width and stress ratio, respectively, at the intersection points in the material model shown in Figure 3.3. The variations in the structural response seen in Figure 3.4 were obtained by varying w_1, w_2 and α_2 within the given intervals. For more details, see Sjölander et al. [102].

3.3 Modelling of bond strength

Two common methods to model contact is the *augmented Lagrange method*, and the *penalty method*. In both models, the contact between two surfaces is modelled using a stiff spring that resolves the contact stresses [35]. The primary difference between the two models is that the penalty method changes the stiffness of involved degrees of freedom (d.o.f), while the augmented Lagrange method adds d.o.f to solve the contact problem [36]. In this report the penalty method has been used to model the interface between shotcrete and rock. The penalty method is implemented in many FE softwares. In Comsol Multiphysics 5.4 [35] and Abaqus [1], the separation of the interface can be modelled using a damage function.

Bond failure was included in the studies presented in [101; 102], but was not the main focus. Details regarding the modelling of the interface are presented in [101; 102]. In a paper by Sjölander et al. [106], the main focus was to understand how the variations in bond strength affect the structural behaviour of shotcrete in interaction with rock. The bond was also an important parameter for the study presented in [105]. Therefore, more focus was put on modelling failure of the interface correctly. The numerical model used by Sjölander et al. [105; 106] is presented below. While many papers are devoted to experimental testing of the interface strength [21; 78; 93; 109], few are devoted to modelling or measurements of the fracture process during interface failure, see e.g. Dong et al. [39; 37; 38].

Modelling of the interface was based on zero-thickness elements, as proposed by Camnaho et al. [25]. This means that the interface is not modelled with separate elements. Instead, the nodes along both sides of an interface are connected with stiff springs. Thus, with the penalty method and an isotropic damage model, the stress σ_{i} and separation u_{i} along the interface is defined by the penalty stiffness K_{i} and the damage scalar ω_{b}.

$$\sigma_{\mathrm{i}} \;=\; K_{\mathrm{i}} u_{\mathrm{i}} (1 - \omega_{\mathrm{b}}) \tag{3.14}$$

To completely define the elastic behaviour of the interface, the compressive K_{Ic}, tensile K_{It} and shear K_{II} stiffness of the interface must be determined. With a model based on stiff springs, a displacement of the interface is required to generate stress. Therefore, a penetration of the contact surface is required to generate a contact pressure. The compressive stiffness K_{Ic} is therefore arbitrarily selected and given a high value to decrease the physical error of the solution, i.e. the penetration of the surfaces. In this report, only Mode-I, i.e. tensile failure, was considered. The reason for this was that for the studied cases, Mode-I stresses are dominating. For the modelling of Mode-I failure, K_{It} should if possible be based on experiments. According to results by Saiang [93] and Dong et al. [38; 39], failure of the interface initiates at a displacement u_{I0} in the range from 0.005 to 0.010 mm, while the bond strength σ_{If} varied between 0.8 and 2.8 MPa [93; 39; 38]. Based on Eq. (3.15), the tensile interface stiffness K_{It} for the tests varied between 159 and 900 GPa/m.

$$K_{\mathrm{It}} \;=\; \frac{u_{\mathrm{I0}}}{\sigma_{\mathrm{If}}} \tag{3.15}$$

Until the failure stress σ_{If}, there is a linear relationship between stresses and displacements. Then, softening occurs until the two interfaces becomes completely separated. An isotropic damage model was used together with the cohesive crack model. Based on experimental results from Dong et al. [37; 38; 39], the relationship between tensile bond stress σ_{It} and separation u_{It} along the interface was described with an exponential function:

$$\sigma_{\mathrm{I}}(u_{\mathrm{I}}) \;=\; \sigma_{\mathrm{If}}\mathrm{exp}\left(\frac{u_{\mathrm{I0}} - u_{\mathrm{I}}}{u_{\mathrm{If}}}\right) \tag{3.16}$$

Here, u_{If} determines the shape of the exponential softening function and depends on the relationship between u_{I0} and the fracture energy G_{If} and tensile bond strength σ_{If} of the interface, according to:

$$u_{\mathrm{If}} \;=\; \frac{u_{\mathrm{I0}}}{2} + \frac{G_{\mathrm{If}}}{\sigma_{\mathrm{If}}} \tag{3.17}$$

The damage function of the interface $\omega_{\mathrm{b}}(u_{\mathrm{I}})$ was derived by setting Eqs. (3.14) and (3.16) equal, which yields:

$$\omega_{\mathrm{b}}(u_{\mathrm{I}}) \;=\; 1 - \frac{u_{\mathrm{I0}}}{u_{\mathrm{I}}}\mathrm{exp}\left(\frac{u_{\mathrm{I0}} - u_{\mathrm{I}}}{u_{\mathrm{If}}}\right) \tag{3.18}$$

An experimental study by Dong et al. [39] was used to verify the numerical model. In the test, concrete was cast against a rock beam and after 28 days of hardening, a notch was sawn through the interface and the beam was subjected to three-point bending until failure. The height h of the beam was 100 mm, and the notch n varied in steps of 10 mm, from 20 to 60 mm, respectively. During testing, the vertical force and the CMOD were measured. A 2D numerical model was created to simulate the experimental results. One fixed and one roller support was used as presented in Figure 3.5, and the load was applied as a controlled displacement. More details are presented in [38; 39] and in [106]. In Table 3.2, the range in mechanical properties of the interface used in the simulations are presented. In Figure 3.5, the simulated and experimental results are compared for five different notch heights. The peak load descended with an increased notch height, i.e. the maximum and minimum force corresponds to a notch height of 20 and 60 mm, respectively.

Table 3.2: Mechanical properties used in the numerical simulations for the interface. From Sjölander et al. [106].

K_{It} **[GPa/m]**	σ_{If} **[MPa]**	G_{If} **[N/m]**
500-600	1.8-2.7	10-25

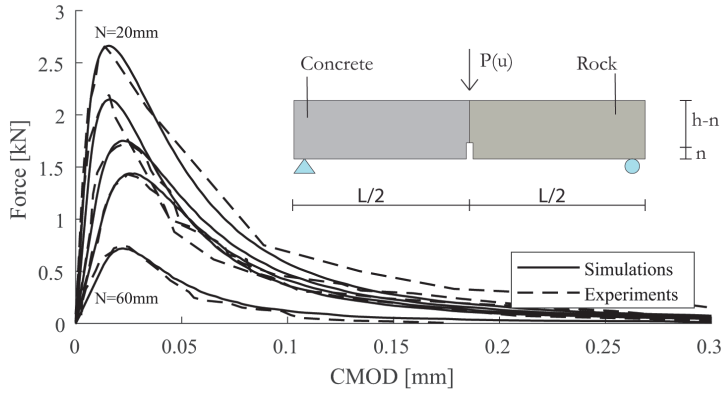

Figure 3.5: Relationship between vertical force and CMOD for notched concrete-rock beams. Numerical simulations with solid lines and experimental results from Dong et al. [39] with dashed lines.

3.4 Modelling of rock bolts

In the paper by Sjölander et al. [105], a numerical model for a grouted rock bolt was presented and used to simulate the structural behaviour of a bolt-anchored shotcrete lining. For a grouted rock bolt subjected to a tensile force, two failure models can be considered; tensile failure, i.e. rupture of the bolt, and pull-out failure of the bolt. It was shown by Li et al. [72] that tensile failure commonly occurs in bolts with an anchorage length of 250 mm or more. In this case, failure is normally preceded by large deformation and some increase in force until rupture occurs. Bolts with a shorter anchorage length than 250 mm, fail more frequently due to pull-out failure [72]. In this report, the structural behaviour of a ribbed steel bar with an anchorage length of less than 100 mm was studied. Based on tests [72], it is reasonable to assume that the bolt will fail due to pull-out. Therefore, an elastic-perfectly plastic material model was used to simulate the structural behaviour of the rock bolt in [105]. In this model, there is a linear relationship between stress and strain until the yield limit of the steel. Thereafter, the stress in the steel was constant.

During pull-out failure, the bolt will slide either along the rock-grout or bolt-grout interface. Commonly, the latter failure dominates [17; 82]. The resistance to pull-out failure is mainly due to friction along the grout-bolt interface, and mechanical interlocking between the ribs and grout. During pull-out, local crushing or cracking of the grout must occur around the ribs of the bolt. In [105], the rock bolt was modelled using solid elements but the ribs were not included. The grout was not explicitly modelled, and the interface was modelled with the same concept as for bond failure, see Section 3.3. However, the pull-out force will cause shear stresses

σ_{II} along the grout-bolt interface and a pure Mode-II, i.e. shear failure mode was assumed.

$$\sigma_{\mathrm{II}} \;=\; K_{\mathrm{II}} u_{\mathrm{II}} (1 - \omega_{\mathrm{II}}) \tag{3.19}$$

A linear relationship between σ_{II}, the shear penalty stiffness K_{II} and the shear slip u_{II} is assumed until the shear strength is reached. As the shear strength σ_{IIf} is reached, failure initiates and the relationship between damage and slip $\omega_{\mathrm{II}}(u)$ is described with a polynomial damage law based on mixed-mode displacement u_{m} [35], according to:

$$\omega_{\mathrm{II}}(u_{\mathrm{m}}) \;=\; \min\left(1, \max\left[0, \frac{u_{\mathrm{m0}}}{u_{\mathrm{m}}}\left(1 + \left(\frac{u_{\mathrm{m}} - u_{\mathrm{m0}}}{u_{\mathrm{mf}} - u_{\mathrm{m0}}}\right)^2\right)\left(2\left(\frac{u_{\mathrm{m}} - u_{\mathrm{m0}}}{u_{\mathrm{mf}} - u_{\mathrm{m0}}} - 3\right)\right)\right]\right) \tag{3.20}$$

This damage law is based on mixed-mode displacement u_{m} with u_{m0} and u_{mf} being the displacement at initiation and complete failure, respectively. The mixed-mode displacements are evaluated based on the Mode-I, u_{I} and Mode-II, u_{II} displacements, as:

$$u_{\mathrm{m}} = \sqrt{(u_{\mathrm{I}}^2 + u_{\mathrm{II}}^2)} \tag{3.21}$$

Compared to the shear stress, the normal stress along the grout-bolt interface will be negligible during pull-out failure. Therefore, the stress-free displacement of the interface u_{mf} was assumed to only depend on the stress-free displacement in the shear direction u_{IIf}. This is calculated based on the relationship between shear fracture energy and failure stress, G_{IIf} and τ_{IIf}, respectively.

$$G_{\mathrm{IIf}} \;=\; \frac{u_{\mathrm{IIf}} \tau_{\mathrm{IIf}}}{2} \tag{3.22}$$

The principle for the test set-up used by Li et al. [72] is shown to the right in Figure 3.6. Holes were drilled into a concrete block, and rock bolts were anchored using grout with a water-cement (w/c) ratio between 0.40 and 0.50. The embedded length varied between 100 and 400 mm. To the left in Figure 3.6, the relationship between relative shear stress and slip for the numerical model is shown for a simulation of pull-out failure for a rock bolt anchored 100 mm. Pull-out failure of rock bolts anchored 100 mm and with three different w/c-ratios; 0.40, 0.46 and 0.50, respectively, were simulated. The range in mechanical parameters are presented in Table 3.3. In Figure 3.7, a comparison between experimental results from [72] and numerical simulations is shown. The aim with the numerical model was to capture the average behaviour for the three tested bolts in respectively test serie.

Table 3.3: Mechanical properties used in the numerical simulations for the rock bolt.

K_{II} **[GPa/m]**	σ_{IIf} **[MPa]**	u_{IIf} **[mm]**	G_{IIf} **[kN/m]**
500-600	6.5-12.0	20-35	97-140

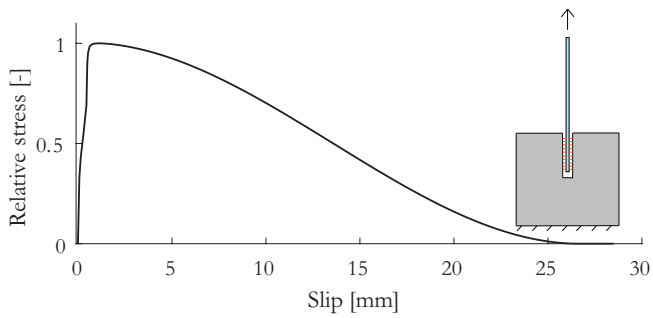

Figure 3.6: Simulated relationship between relative shear stress along the bolt-grout interface and shear slip during pull-out failure.

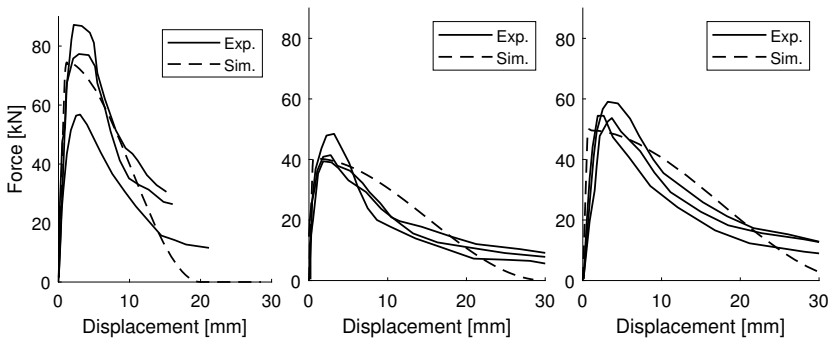

Figure 3.7: Relationship between pull-out force and vertical displacement for a rock bolt anchored 100 mm in concrete with varying w/c-ratio. From left to right, the w/c-ratio was 0.40, 0.46, and 0.50, respectively.

3.5 Modelling of drying shrinkage

To account for the effects of non-linear drying along the thickness of the shotcrete, a model based on multi-physics was used to simulate drying shrinkage by Sjolander and Ansell Sjölander et al. [104]. With a multi-physics model, the governing equations for different physical fields such as; temperature, moisture transportation and mechanical strain can be solved simultaneously, and also be given a coupled behaviour. An extensive review of the concept and applications of coupled multi-physical models is presented by e.g. Gasch [45; 46] and Indiart [65]. Using this concept, the drying process of shotcrete was described as a pure diffusion process. This means that all water transportation occurs in the vapour phase. In the model, this process was driven by the gradient in relative humidity $\Delta\phi$, and the flux J, i.e. the change in relative humidity over the area, was described by Fick's first law:

$$J = -D_{\mathrm{H}} \cdot \Delta\phi \tag{3.23}$$

Here, D_{H} is the coefficient of diffusivity for the shotcrete, which describes the rate of moisture transportation. This is, according to Bazant and Najjar [12], a non-linear function which depends on the relative humidity H in the shotcrete.

$$D_{\mathrm{H}} \;=\; -D_1 \left[\alpha_0 + \frac{1-\alpha_0}{1+\left(\frac{1-H}{1-H_{\mathrm{c}}}\right)^n} \right] \tag{3.24}$$

When the relative humidity is equal to 1 and 0, i.e. 100 % and 0 %, the diffusivity is described by D_1 and D_0, respectively. The relationship between D_1 and D_0 is described with α_0, according to:

$$\alpha_0 \;=\; D_0/D_1 \tag{3.25}$$

When H approaches H_{c}, the diffusivity suddenly changes several orders of magnitude. The rate of change is described by the parameter n in Eq. (3.24). The change in relative humidity described by Fick's first law, Eq. (3.23), is valid for steady-state conditions. For a transient event, such as drying of shotcrete, Fick's second law must be used:

$$\frac{\partial H}{\partial t} \;=\; D_{\mathrm{H}} \nabla \phi \tag{3.26}$$

The partial derivative $\partial H/\partial t$ describes the change in relative humidity over time, which depends on the second derivative of the relative humidity, $\nabla\phi$ multiplied with D_H. A boundary condition, describing the exchange in moisture between the shotcrete surface and ambient air, is needed to complete the moisture transportation model. A boundary condition specifies the solution to the differential equations along the boundaries. Different types of boundary conditions, and their impact on the solution to the moisture transportation problem, are:

- First type of boundary condition, Dirichlet boundary condition. This specifies the value of H along the boundary.
- Second type of boundary condition, Neumann boundary condition. This specifies the value of the derivative H' along the boundary.
- Third type of boundary condition, Robin boundary condition. This specifies the value along the boundary using a linear combination of H or H'.

Here, a Robin boundary condition was used to describe the flux J along the boundary. This was driven by the difference in relative humidity between the surface H, and ambient air H_{env}, multiplied with the surface factor β_{h}, which describes the rate of exchange in moisture between the surface and ambient air. Finally, N in Eq. (3.27) is the normal to the surface.

$$-\,J \cdot N \;=\; \beta_{\mathrm{h}} \cdot (H - H_{\mathrm{env}}) \tag{3.27}$$

Chapter 4

Results

In this chapter, important results from this research project are presented. First, a short introduction to the studied load case is given. Then, the most important aspects of the numerical model is presented. Further details regarding the numerical models can be found in Chapter 3 and in given references.

4.1 In-situ variations of shotcrete

As presented in Sections 2.3 and 2.4, variations in mechanical strength, bond strength and thickness of in-situ shotcrete exist. In the work by Bjureland et al. [16], a unique set of data was analysed in order to quantify the distribution of these parameters. The shotcrete should fulfil the requirements for C32/40 according to EN 1992-1-1 [28] and the mix is presented in Table 4.1.

Table 4.1: Mix of shotcrete used for material testing. From Bjureland et al. [16].

Material	**Content [kg/m^3]**	**Unit**
Cement CEM I 42.5 N-SR 3 MH-LA	520	[kg/m^3]
Water	208	[kg/m^3]
Water/cement ratio	0.4	[-]
Steel fibres	55	[kg/m^3]

4.1.1 Mechanical strength of shotcrete

In Bjureland et al. [16], the flexural $f_{\mathrm{ctm,fl}}$ and residual flexural $f^{\mathrm{re}}_{\mathrm{ctm,fl}}$ strength of the shotcrete were evaluated based on four-point bending tests according to EN 14488-3 [30]. In total 344 beams were tested. The compressive strength was evaluated based on cubes according to EN 12504-1 [33]. A total of 690 cubes were tested. Specimens were extracted from shotcrete slabs which were sprayed and cured in-situ. The mean, standard deviation (std) and 5 percentile (5%) values from in-situ testing of $f_{\mathrm{ctm,fl}}$, $f^{\mathrm{re}}_{\mathrm{ctm,fl}}$ and f_{c} for the shotcrete are presented in Table 4.2. Furthermore, the 5 percentile for a C32/40 concrete according to EN 1992-1-1 [28] is presented. Here, the thickness of the shotcrete was considered while determining the flexural strength. The requirements for the project are also given in the table. The requirements for $f_{\mathrm{ctm,fl}}$, $f^{\mathrm{re}}_{\mathrm{ctm,fl}}$ and f_{c} are based on the mean value of a test series of three samples. Moreover, a requirement of the individual strength of $f_{\mathrm{ctm,fl}}$, $f^{\mathrm{re}}_{\mathrm{ctm,fl}}$ is also specified. Clearly, the tested shotcrete fulfilled the project requirements. A histogram and probability density function for the test data are shown in Figure 4.1. As can be seen, the variation in material strength can be relatively well described with a normal distribution.

Table 4.2: Tested mechanical strength for shotcrete and requirements according to EN 1992-1-1 [28] for a C32/40 concrete and project requirements. From Bjureland et al. [16].

Strength	**Samples**	**In-Situ [MPa]**			**EN 1992-1-1**	**Requirement**
		mean	**std**	**5%**	**5%[MPa]**	**mean[MPa]**
Compressive	690	59	8.1	45	40	40^{b}
Flexural	344	6.8	0.8	5.4	3.3	3.2^{a} / 4.0^{b}
Residual flexural	344	3.8	0.8	-	-	2.4^{a} / 3.0^{b}

a= Individual test b= Average of test series

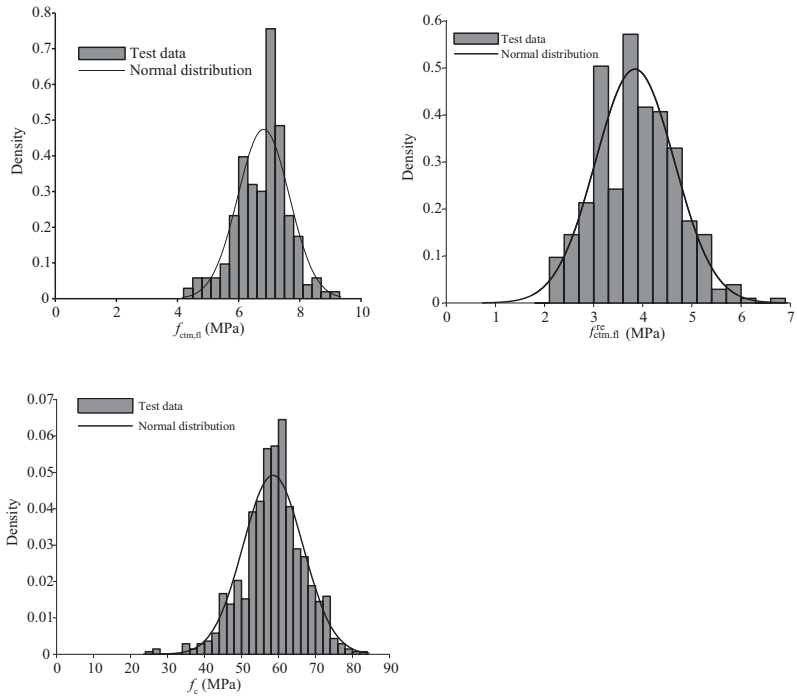

Figure 4.1: Examples of in-situ variations in flexural $f_{\mathrm{ctm,fl}}$, residual flexural $f^{\mathrm{re}}_{\mathrm{ctm,fl}}$ and compressive strength f_{c} strength of fibre reinforced shotcrete. From Bjureland et al. [16].

The bond strength was evaluated according to EN 14488-4 [32], which means that the bond is tested through direct tension. Tests are performed on drilled cores with a diameter between 50 and 100 mm that are extracted after a minimum of 28 days of curing. The mean value of a test series of three samples should according to the project requirements exceed 0.5 MPa. A total of 354 samples of bond strength were analysed. The probability density function and histogram for the bond strength between shotcrete and rock (granite and gneiss) are presented to the left in Figure 4.2. The mean and standard deviation for the bond strength were 0.81 and 0.32 MPa, respectively. Moreover, the data have been divided into subsets depending on the mapped failure surface. It should be noted that a majority of the failures with a bond strength $\leq$ 0.5 MPa occurred to 50% or more in the rock mass. As shown by Malmgren et al. [78], removing the rock mass with low strength before spraying is one way to reduce the risk of achieving low bond strength. To the right in Figure 4.2, the measured bond strength between shotcrete and granite or gneiss is plotted together with the corresponding Rock Mass Rating (RMR) value. This shows that no correlation exists between bond strength and RMR, which has been proposed by e.g. Brady et al. [18].

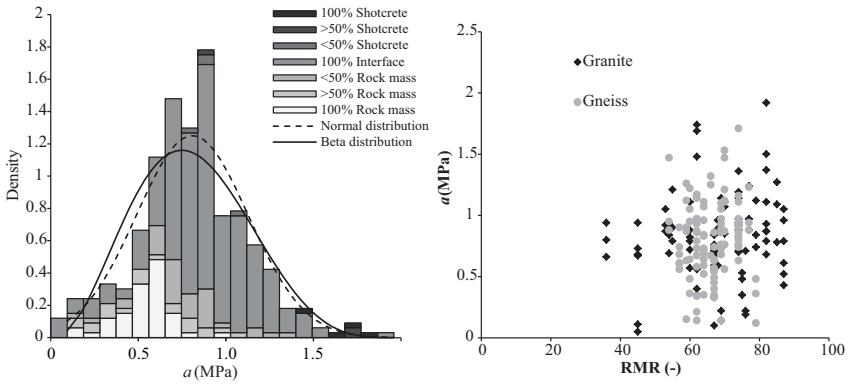

Figure 4.2: To the left, probability density function for the bond strength between shotcrete and rock divided into subsets depending on the mapped failure surface. To the right, measured bond strength for granite and gneiss and the corresponding RMR value. From Bjureland et al. [16].

4.1.2 Shotcrete thickness

The shotcrete thickness was evaluated according to EN 14488-6 [31] and data from more than 6000 drilled holes were analysed. According to the project requirements, the mean value of a test series of five samples should exceed the required thickness. Furthermore, all individual samples should exceed 80% of the required thickness. The histogram and probability density functions for the shotcrete thickness are presented in Figure 4.3. First, data for three cases with a required thickness of 50, 75 and 100 mm are presented. A log-normal distribution was found to describe the data from all tests rather well. From Figure 4.3 it can be seen that too much shotcrete is generally used but that sections with too low thickness also exist. To the left in Figure 4.4 the cumulative distribution function (CDF) is plotted for the different required thicknesses. The requirements for each case are highlighted which shows that more shotcrete is used in 87, 78 and 68% of the cases when the shotcrete thickness is 50, 75 and 100 mm, respectively. To the right in Figure 4.4, part of the CDF is plotted and the requirements for individual samples, i.e. 80% of the required thickness is highlighted. This shows that for the suggested distributions, the required thickness for an individual sample will not be achieved in 4, 7 and 13% of the cases when the required thickness is 50, 75 and 100 mm, respectively. In Table 4.3, the mean value, standard deviation (std) and coefficient of variation (COV) are presented. Here, it can be seen that the mean value of the shotcrete thickness is around 20 to 30 mm more than the required thickness. One of the reasons to the large variability shown in the data is that it is difficult to estimate the applied thickness. The reason to that the mean value

is 20 to 30 mm higher compared to the required value can probably be explained by economical or practical aspects. Likely, it is better and more economical for the contractor to apply an extra layer of shotcrete during the first round of spraying. If the required thickness is not achieved, an extra layer of shotcrete must be applied, which could cause delays and extra costs in the project. Moreover, there is also a risk that an insufficient bond strength is achieved between the two shotcrete layers which introduces a weak zone.

Table 4.3: Statistical data for shotcrete thickness. From Bjureland et al. [16].

Requirement [mm]	Samples	Mean [mm]	std [mm]	COV [%]
50	2405	81	31	38
75	2040	100	32	32
100	1813	123	42	34

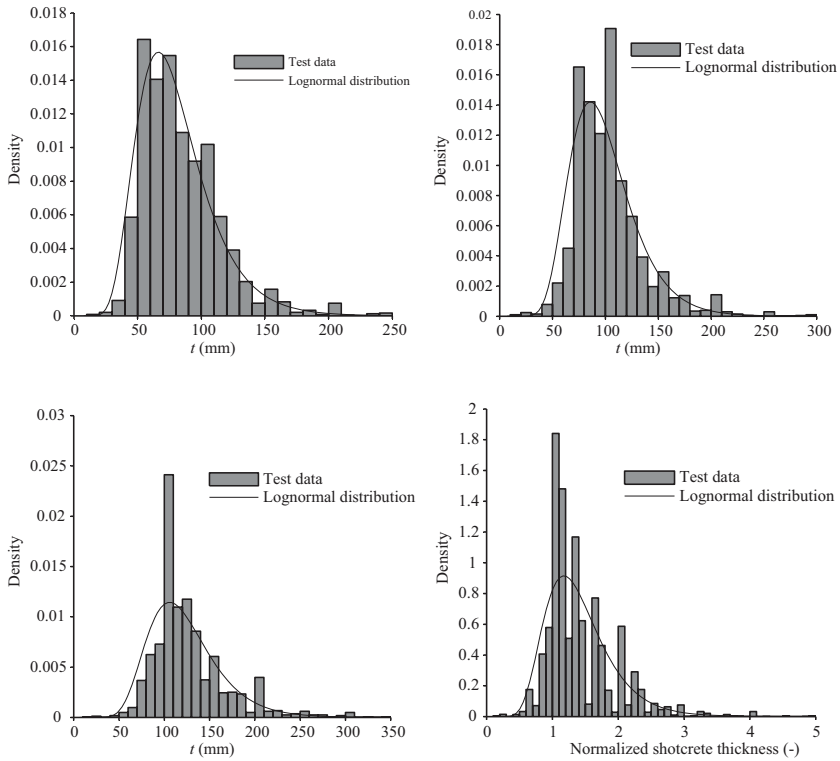

Figure 4.3: From top to bottom, left to right, shotcrete thickness data for a required thickness of 50, 75 and 100 mm as well as all results normalized with respect to the individual required thickness. From Bjureland et al. [16].

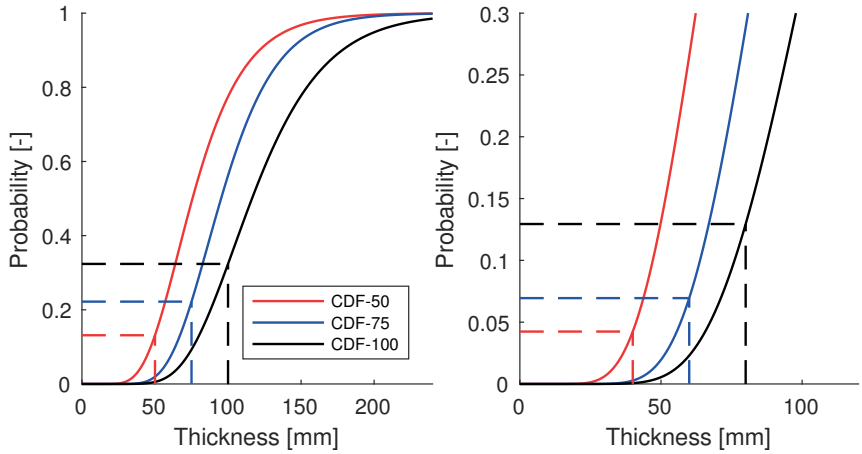

Figure 4.4: Cumulative distribution function (CDF) for shotcrete thickness and highlighted requirements for mean value 50, 75 and 100 mm, respectively. To the right, part of the CDF is plotted together with the requirements for individual thickness.

4.2 Studies on shrinkage loads

Drying shrinkage of a restrained shotcrete lining is a well-known risk factor for cracking and has gained considerable interest from the scientific community. Leung et al. [71] and Bryne et al. [22] presented new test configurations to investigate drying shrinkage for end-restrained specimens, while Banthia et al. [9] studied how different type of fibres influence cracking of fibre reinforced concrete. Failure mapping presented by Malmgren et al. [78], suggested that drying shrinkage was one of the failure mechanisms that caused fall-outs of shotcrete. In most cases, the shotcrete thickness was less than 20 mm. In-situ investigations by Ansell [5] showed that end-restrained shotcrete is prone to shrinkage induced cracking and that, typically, one wide crack forms in each section.

In this report, experimental data from Carlswärd [26] and Bryne et al. [23] were used to study drying shrinkage. The set-up for these studies are shown in Figure 4.5. Both test series were performed in a laboratory environment. In the study by Carlswärd [26], thin concrete beams, with and without fibre reinforcement, were cast on top of a concrete slab, see the left side of Figure 4.5. In the study by Bryne et al. [23], shotcrete was sprayed over a granite slab in which the centric part was covered with plastic sheeting to prevent bonding between shotcrete and rock. Thus, the first tests contain continuously restrained specimen with uniform thickness, while the other tests were performed on end-restrained specimen with varying thickness. More details about the experimental set-ups are given in [101; 102].

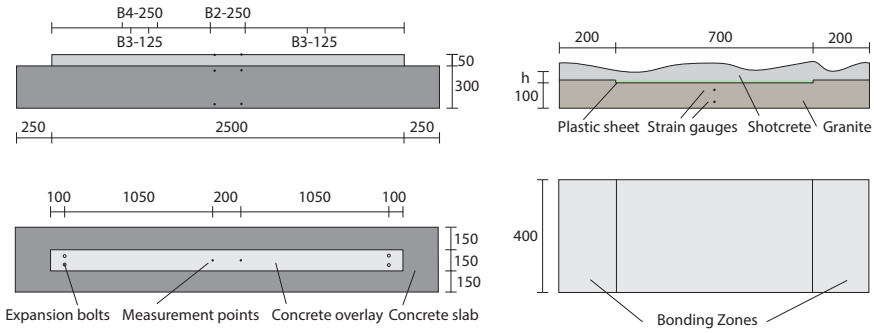

Figure 4.5: Experimental set-up for verification of the FE model from Carlswärd [26] (left) and to study the influence of a varying thickness, from Bryne et al. [23] (right).

4.2.1 Effects of partial bond failure between shotcrete and rock

In Section 4.1.1, it was shown that the bond strength can vary significantly, and that areas with low or zero bond strength exist in a tunnel. How such areas affect the cracking of the shotcrete when it is subjected to shrinkage was studied by Sjölander and Ansell [101]. A FE model was created in the software Abaqus [1]. A bi-linear softening curve, verified against experimental results, was used to simulate the structural behaviour of glass fibre-reinforced shotcrete. The used fibre was a microfibre which has no practical effect on the ductility of the shotcrete. Thus, shotcrete was modelled as unreinforced. The interface between shotcrete and rock was modelled with the penalty method as described in Section 3.3. The interface stiffness was set equal to ten times a representative underlying element stiffness, which is the default stiffness [1]. Shrinkage was considered to be uniform and modelled as a linearly decreasing temperature. Experimental results from Carlswärd [26] were used to verify the structural behaviour of the numerical model. More specifically, the aim was to show that the numerical model could capture the different crack patterns for fully and partially bonded overlays. The set-up is shown to the left in Figure 4.5 and consists of a 2500 $\times$ 150 $\times$ 50 mm (length $\times$ width $\times$ height) concrete overlay cast against a concrete slab. After casting and initial curing, the overlays were subjected to drying in a laboratory environment. More details are given in [101].

In Figure 4.6 a), selected results from Carlswärd [26] show that a systematic pattern of fine cracks forms in unreinforced concrete with a continuous bond to a substrate. However, few and wide cracks form when the bond is lost. To investigate the effect of partial bond failure, some areas were modelled without bond to the substrate. These areas are highlighted as "debonding prior analysis" in Fig-

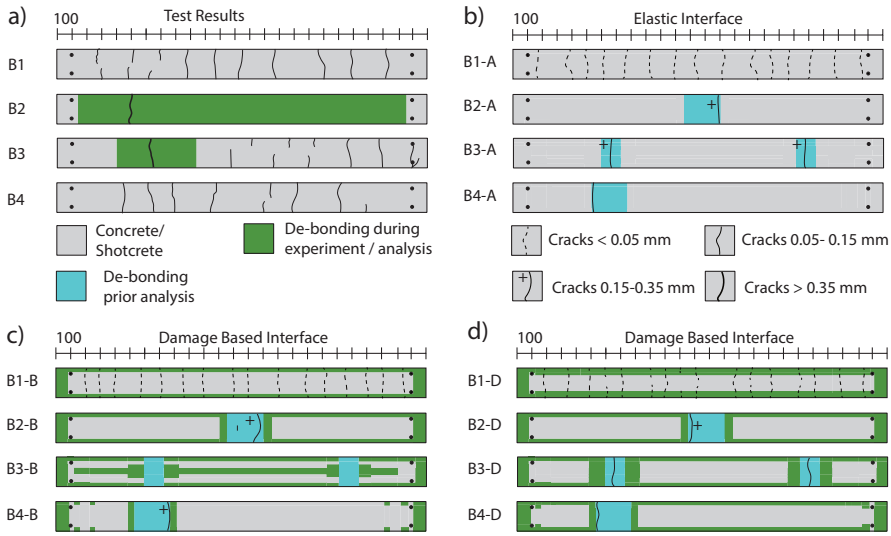

Figure 4.6: Crack patterns and bond failure for thin beams B1-B4 cast on concrete slabs. In a), selected experimental results from Carlswärd [26] and b)-d), numerical simulations from Sjölander and Ansell [101]. The interface was modelled in b), as linear elastic and in c)-d), with a softening law with a fracture energy of 125 and 10 Nm, respectively.

ure 4.6. For the results shown in b), an elastic interface was used which means that no failure can occur. These results show that the numerical model was able to simulate the behaviour from the experiments. Moreover, it shows that wide cracks form when a small area lacks bond to the substrate. The results in Figure 4.6 c)-d) compare crack patterns and the propagation of bond failure when the fracture energy of the interface G_{If} was 125 and 10 Nm for c) and d), respectively. The crack formations correspond well to experimental results, but bond failure occurred mainly around the perimeter of the overlay in the simulations. This was not the case in the experiment. Possibly, the simulated bond failure was initiated by shear stresses, which for a fully restrained beam will have a maximum value around the perimeter, see e.g. Silfwerbrand [96]. Thus, the reason for the mismatch in bond failure propagation could be that the bond shear strength τ_{II}, which was set to 3.0 MPa, was not correctly assumed.

4.2.2 Effects of varying shotcrete thickness

Bryne et al. [22] presented a new test set-up to investigate the effects of shotcrete subjected to end-restrained shrinkage, which is shown to the right in Figure 4.5. The set-up consisted of a sawn granite slab covered with a layer of shotcrete. A

centric area of the slab was covered with plastic sheets to prevent bonding. This created conditions similar to when shotcrete is sprayed against drain-mats. This set-up was used to investigate if the addition of micro glass fibres in the shotcrete could prevent the formation of drying shrinkage cracks [23]. A total of six slabs were sprayed and subjected to drying in a climate chamber. A mechanical instrument was used to measure the thickness of the shotcrete in a basic grid pattern of 50×10 mm.

Numerical simulations of these experiments were performed to investigate how the variations in thickness will affect the localization of cracks in the shotcrete. The same material and interface model for shotcrete as described in Chapter 4.2.1 was used. However, only an elastic material model was used to describe the interface. The measured data were used to model the variations in shotcrete thickness. The effect of drying shrinkage was here modelled as a uniform shrinkage. Two cases were considered; in the first, shotcrete was end-restrained as in the experiments [23], and in the second case, shotcrete was continuously restrained to the

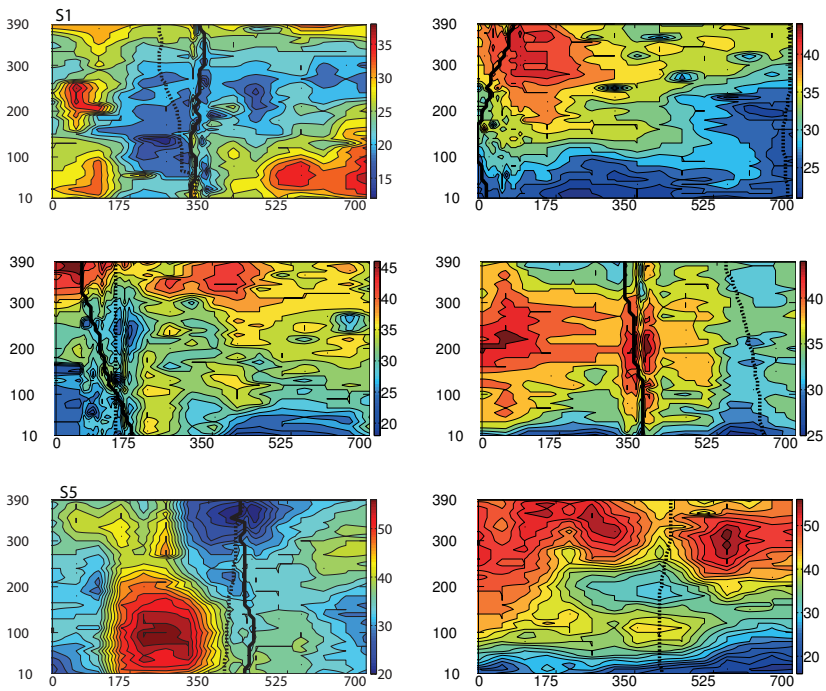

Figure 4.7: Formation of cracks in an end-restrained slabs and their location with respect to minimum (blue) and maximum (red) thickness for slab S1 to S6 (left to right, top to bottom). Solid and dashed lines show experimental and numerical results, respectively. From Sjölander and Ansell [101] and Sjölander [100].

rock surface. Results from case one and two are presented in Figures 4.7 and 4.8, respectively. A contour plot shows the variations in shotcrete thickness between the two bonding zones, as indicated to the right in Figure 4.5. Simulated cracks are plotted with dashed lines, while cracks from the experiments are plotted with solid black lines. Only cracks wider than 0.05 mm are plotted.

For the end-restrained slabs shown in Figure 4.7, one through crack formed and propagated along the width to finally separate the slab into two parts. After cracking, the slabs were fully unloaded and no other cracks formed. The variations in shotcrete thickness will cause a disturbance in the stress flow, which introduces stress concentrations. Furthermore, local changes in thickness introduces stresses due to bending. The simulated crack patterns in Figure 4.7 highlight, theoretically, the preferable crack patters in the slab. Theses sections have either low stiffness or more abrupt changes in geometry. In practice, other factors such as variations in shotcrete strength, unfavourable distribution of large aggregates and defects in the shotcrete affects the formation of cracks. These factors are possible expla-

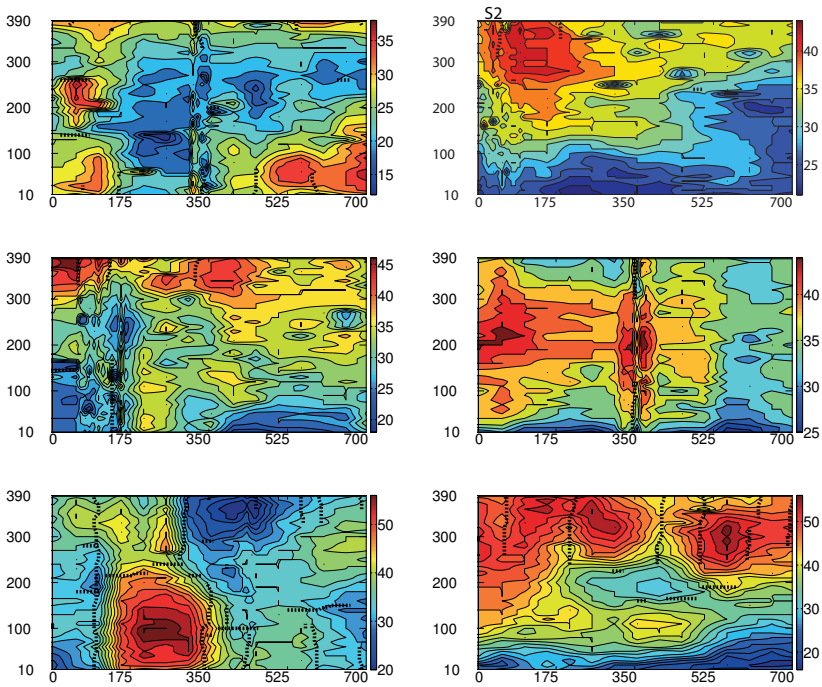

Figure 4.8: Simulated cracking of continuously restrained slabs and their location with respect to minimum (blue) and maximum (red) thickness for slab S1-S6 (left to right, top to bottom). From Sjölander and Ansell [101] and Sjölander [100].

nations for the deviations in crack patterns between experiments and simulations that are seen for Slabs 2 and 4. It should be noted that in the experiment, Slab 6 failed due to debonding and no cracks formed.

The crack patters for the continuously restrained shotcrete slabs with varying thickness are presented in Figure 4.8. As can be seen, multiple cracks formed but most of them did not propagate along the full thickness of the shotcrete. This is similar to the structural behaviour of reinforced shotcrete. However, the micro glass fibres used to reinforce the shotcrete has no measurable effect on the ductility. Therefore, it is evident that the bond between shotcrete and rock will redistribute forces and prevent major cracks from forming. It was shown by Groth [48] that the thickness of the overlay, i.e. in this case the shotcrete, affects the cracking and that a finer distribution of cracks are formed for thinner overlays. In Figure 4.8, it can be seen that more cracks are formed in a slab with more abrupt changes in thickness, S5, or in a slab with larger thickness, S6. In cases with more moderate changes in thickness, fewer or more narrow cracks seems to form.

4.2.3 Non-linear drying shrinkage for end-restrained shotcrete

When shotcrete dries, free capillary water is transported to the surface of the shotcrete from which it evaporates to the ambient air. The rate of water transportation within the shotcrete depends largely on the thickness, but also on the pore system. The main driving force for water transportation is the change in relative humidity (RH) between the shotcrete and the ambient air. The rate of drying from a surface depends on the ambient air, e.g. wind speed and RH of the air. For a shotcrete lining, drying is one-sided and the variations in thickness lead to local differences in drying. This results in strain gradients through the shotcrete. How non-linear drying shrinkage affects the cracking of shotcrete was investigated by Sjölander and Ansell. [102]. The experimental set-up by Bryne et al. [23], as described above, was used. The reason for using this experiment was that the necessary data for the simulations were available and that the tests were performed under controlled environmental conditions. This data contained continuous measurements of strain until the shotcrete cracked, as well as data from free shrinkage testing. Strain gauges were placed close to the upper and lower edge of the granite slab as shown to the right in Figure 4.5. The glass fibre-reinforced shotcrete was modelled as unreinforced shotcrete using the damage model described in Section 3.2, while the bond between shotcrete and rock was modelled with the penalty method, as described in Section 3.3. Drying shrinkage of the shotcrete was modelled with the multi-physical approach described in Section 3.5. First, data from a shrinkage test were used to find an approximate relationship between loss of moisture and mechanical shrinkage. Then, numerical simulations of the drying shrinkage experiments by Bryne et al. [23] were performed. Here, six end-restrained shotcrete slabs with varying thickness were

subjected to drying. The aim was to see if the time to failure could be simulated, and to investigate if non-linear drying affects the cracking of shotcrete. In Table 4.4, the amount of glass fibre-reinforcement, time to failure in the experiment and simulations as well as the minimum, maximum and mean shotcrete thickness are presented for all slabs.

In Figure 4.9, experimental results from Bryne [20] and Sjölander and Ansell. [102] are presented. Here, it is clear that the numerical model was unable to predict the time to failure for the shotcrete slabs. Most of the slabs in the experiment failed after six to seven days of drying, while failure for the simulated slabs occurred after 11 to 18 days. Thus, the rate of drying or the relationship between loss in moisture and mechanical strain was underestimated in the model. Below, some possible reasons for the mismatch between simulations and experiments are listed:

- Parameters for the moisture transportation model were selected to fit experimental results from free shrinkage test. This was performed on shotcrete beams that were cured for three days under water, while the slabs were cured for three days under a wet cloth. This could have affected the hydration and porosity of the specimens.
- During the free shrinkage tests, reliable measurements of strains were obtained first after six days of hardening. This means that the parameters for the moisture transportation model were chosen to fit the rate of drying for a specimen cured for six days and then used to simulate the rate of drying for a specimen cured for three days.
- Both experiments were performed using the same shotcrete mix. However, the free shrinkage tests were performed on cast beams, while the end-restrained tests were using sprayed slabs. Therefore, the air content and the compaction could differ between the two samples which may effect the rate of drying.

Table 4.4: Amount of glass fibre reinforcement, time at failure due to shrinkage and measured thickness for Slab 1-6.

Slab	**Fibres**	**Time of Failure [d]**		**Thickness [mm]**		
	[kg/m^3]	**[Test]**	**[FEM]**	**Min / Max**	**Mean**	**St.D**
S1	0	6-C	11-C	12 / 38	25	5
S2	0	7-CS	15-CS	21 / 45	33	6
S3	5	6-C	15-CS	19 / 48	32	5
S4	5	16-C	16-C	25 / 45	37	4
S5	10	7-C	13-C	20 / 58	37	7
S6	10	6-B	18-C	17 / 57	41	9

B = Bond failure, C = Cracking between bond zone, CS = Crack along bond zone

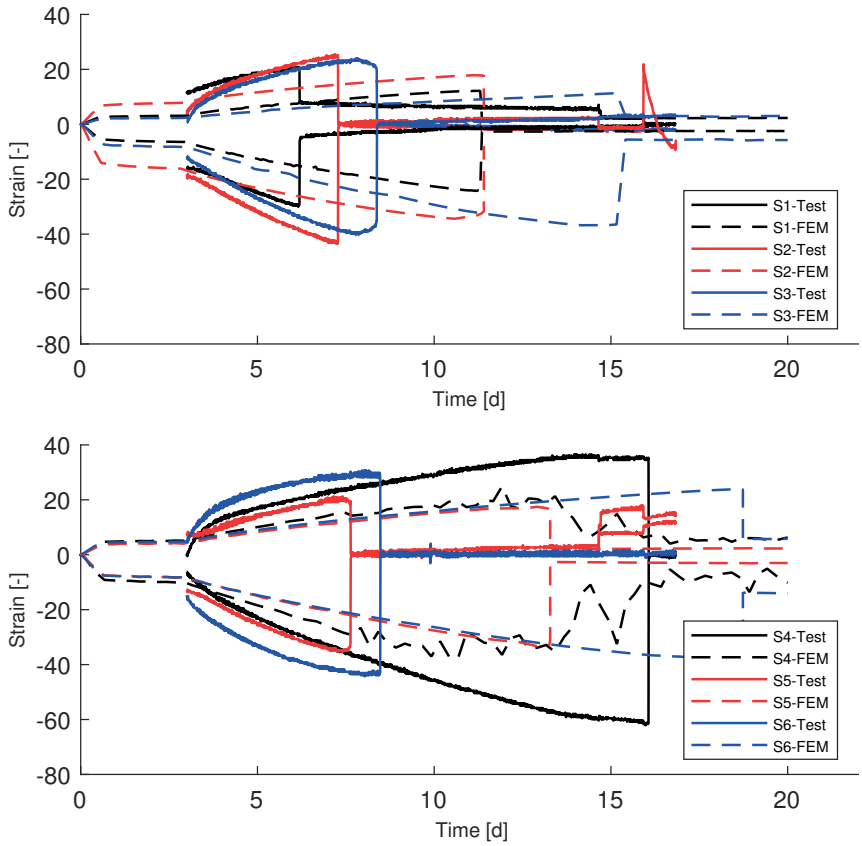

Figure 4.9: Experimental and numerical results from [20] and Sjölander and Ansell. [102] for slabs 1-3 (top) and slabs 4-6 (bottom). Experimental results are plotted with solid lines and simulations with dashed lines.

4.3 Gravity loads from a block

As discussed previously, the general idea is that shotcrete should be able to support the load from a smaller block. Therefore, the gravity load from a loose block is an important load case that should be considered in the design of shotcrete, see e.g. the Swedish Regulations for traffic tunnels [117]. This is one of the reasons to consider this load-case in this report. The other reasons were that the load case is well defined, and that test data were available. Large scale testing of the structural capacity for a shotcrete lining was performed during the 1970s and 1980s by Fernandez-Delgado et al. [42] and by Holmgren [56; 58]. In both studies, three blocks were covered with a layer of shotcrete, see Figure 4.10. After a few days of hardening, a hydraulic jack was used to push the centric block

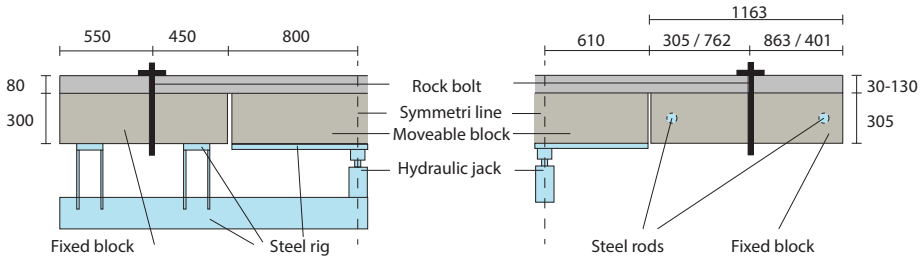

Figure 4.10: From left to right, set-up for experimental testing of structural capacity for shotcrete lining by Holmgren [56; 58] and Fernandez-Delgado et al. [42]. Set-up was symmetric and half of the specimen is shown. Dimensions are given in mm.

through the shotcrete while the required force and vertical displacement of the block were monitored. In the study by Fernandez-Delgado et al. [42], most of the tests were performed on unreinforced shotcrete with varying thickness. The distance between the moving block and rock bolts was also varied [42]. In the study by Holmgren [56; 58], the fibre content and the design of the rock bolt was investigated while the shotcrete thickness for most of the tests was kept equal to 80 mm.

As shown in [16], variations in shotcrete thickness and bond strength can be relatively large in comparison to the values used in design. Moreover, in-situ testing performed during construction of a tunnel will typically show that the required shotcrete thickness, or bond strength, is not fulfilled in certain sections. Today, it is not fully understood how this affects the structural capacity of the lining. More specifically, it is not known if local areas with low bond strength or thickness will govern the structural capacity or not. Furthermore, the conclusion from previous studies [42; 56; 58] is that the structural capacity due to bond failure is unaffected by the thickness in the range from 40 to 140 mm. Therefore, the thickness is commonly neglected in analytical solutions, see e.g. Barrett and McCreath [10]. However, as mentioned in Section 2.2, a linear relationship between the load transfer band δ_b and the shotcrete thickness is suggested in the Swedish design guidelines [118]. For this reason, the influence of local variations in bond strength and thickness with respect to structural capacity is presented below together with a study regarding the failure mechanisms of a bolt-anchored and fibre-reinforced shotcrete (FRS) lining.

4.3.1 Effects of local variations in bond strength

Numerical simulations were performed to study how local variations in tensile bond strength σ_{Ib} between shotcrete and rock affect the structural capacity of the lining. This was done by comparing the maximum force that a shotcrete lining could be subjected to for different cases of varying bond strength. The geometry

from the experiments by Fernandez-Delgado et al. [42] was used, see Figure 4.11. In this figure, δ_{b} represent the length of the interface that is subjected to tensile bond stress, i.e. separation of the interface has initiated. The interface between shotcrete and rock was modelled according to Section 3.3. All in-situ testing of bond strength is based on samples obtained from discrete points. Therefore, the spatial correlation is unknown and a random function was derived to model the variations in bond strength along the shotcrete-rock interface. Further details are given by Sjölander et al. [106]. In total, three cases with different uniform bond strength and twenty cases with local variations in bond cases were studied. The fracture energy of the interface G_{If} was scaled linearly against a reference value of 30 N/m for σ_{Ib}= 0.8 MPa. The bond strength and fracture energy varied in the range from 0 to 1.6 MPa and 0 to 60 N/m, respectively. All translations along the bottom surface of the blocks were restrained. The centric block was defined with a prescribed displacement to push it through the shotcrete.

To the left in Figure 4.12, the relationship between force and vertical displacement of the centric block for three cases with varying uniform bond strength is shown. Naturally, the maximum force increases with an increased bond strength. To understand how the stresses are distributed along the interface at failure, tensile bond stresses are plotted to the right in Figure 4.12. Stresses were plotted at the same time as the peak force shown to the left in Figure 4.12, was reached. The location for which the stresses are plotted is shown in Figure 4.11 and stresses were only plotted over a limited length. Here it can be seen that length of the interface subjected to tensile bond stress is increased for a decreasing bond strength. This means that failure has propagated further, which is a result of a lower fracture energy of the interface since G_{If} was scaled linearly, i.e. $G_{\mathrm{If}} = (\sigma_{\mathrm{Ib}}/0.8[\mathrm{MPa}])\times 30$ [N/m].

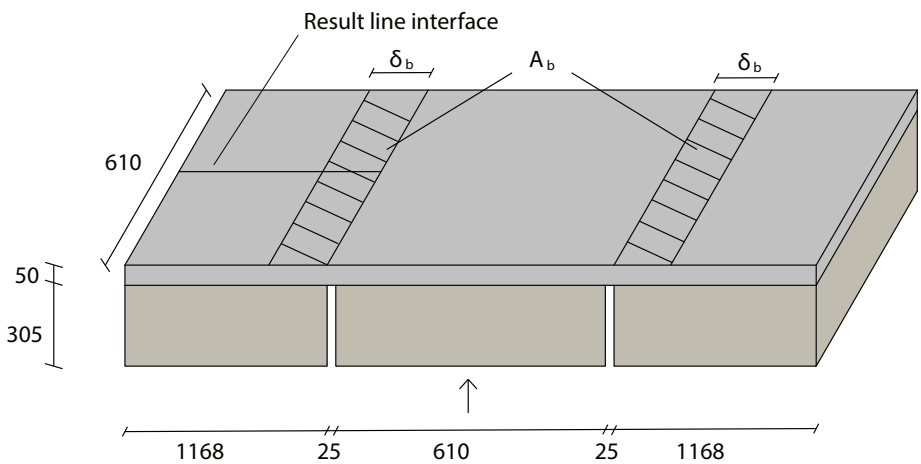

Figure 4.11: Geometry of model used to study the effect of local variations in bond strength and shotcrete thickness. Dimensions are given in mm.

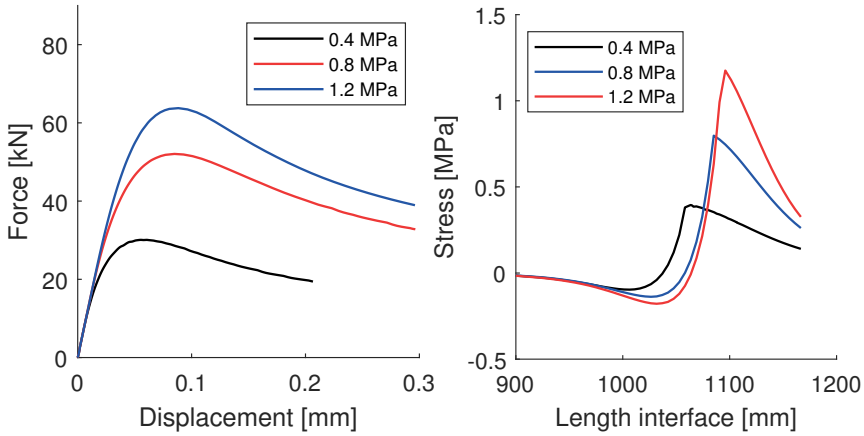

Figure 4.12: The left figure shows the relationship between force and vertical displacement of the centric block for three cases with uniform bond strength. The right figure shows the tensile bond stress along a part of the interface at the moment when the maximum force was reached. From Sjölander et al. [106].

In Figure 4.13, correlations between maximum force $F_{\max}$ and minimum $\sigma_{\mathrm{I,min}}$, mean $\sigma_{\mathrm{I,mean}}$ and maximum $\sigma_{\mathrm{I,max}}$ bond strength in the area subjected to tensile bond stress are shown. This area A_{b} corresponds to the width of the slab multiplied with the length subjected to tensile bond stress δ_{b}, as shown in Figure 4.11. The results in Figure 4.13 show that a strong linear correlation exists between the structural capacity of the lining and the mean value of the bond strength in the area A_{b}. There is no correlation between the structural capacity and the minimum or maximum bond strength for the studied cases. These results indicate that the structural capacity is governed by the mean value of the bond strength around the perimeter of the block, i.e. the area A_{b}. Thus, for the studied distributions of bond strength, local areas with low bond strength are not decisive for the structural capacity.

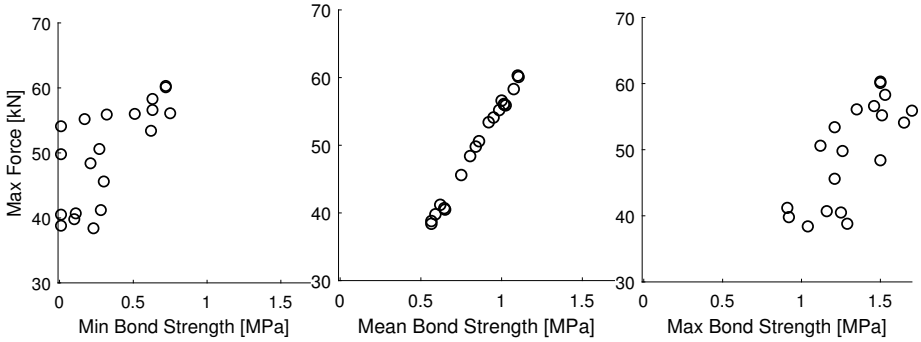

Figure 4.13: Correlations between maximum force and the minimum, mean and maximum bond strength over the area subjected to tensile bond stress for all studied cases with variations in bond strength. From Sjölander et al. [106].

4.3.2 Effects of local variations in thickness

The same geometrical model, as shown in Figure 4.11, was used to study how local variations in thickness affects the structural capacity for a shotcrete lining. In this study, the bond strength σ_{Ib} and fracture energy of the interface G_{If} was uniform and set to 0.8 MPa and 30 N/m, respectively. Results from a 3D laser scanning, i.e. point cloud data, from a tunnel was used to to create a realistic geometry for the shotcrete. These data contain xyz coordinates for the rock surface and the shotcrete surface. For each of the ten models created, a section from the centre of the tunnel roof was selected. In Figure 4.14, contour plots for the shotcrete thickness is plotted for two examples. In addition, five cases with uniform thickness were studied, in the range from 25 to 125 mm. In the numerical model, all translations for the three blocks were restrained along the bottom surface. Then, a vertical displacement was applied to the centric block to push it through the shotcrete lining.

To the left in Figure 4.15, the relationship between force and vertical displacement is plotted for the cases with uniform thickness. Clearly, with an increased shotcrete thickness, the stiffness and structural capacity of the lining also increases. This result is reasonable, since a displacement of the interface must occur to generate stresses and cause bond failure. With the interface between shotcrete and rock modelled with springs, the structural behaviour of the shotcrete depends on the relationship between the interface stiffness K_{I} and shotcrete stiffness K_{s}. If $K_{\mathrm{I}} \ll K_{\mathrm{s}}$, the vertical translation results in a rigid body movement of the shotcrete, and a vertical displacement of the springs. For the opposite, i.e. $K_{\mathrm{I}} \gg K_{\mathrm{s}}$, no translation occurs in the springs and the shotcrete will deform. In the studied case, the vertical translation of the centre block resulted in a vertical displacement of the

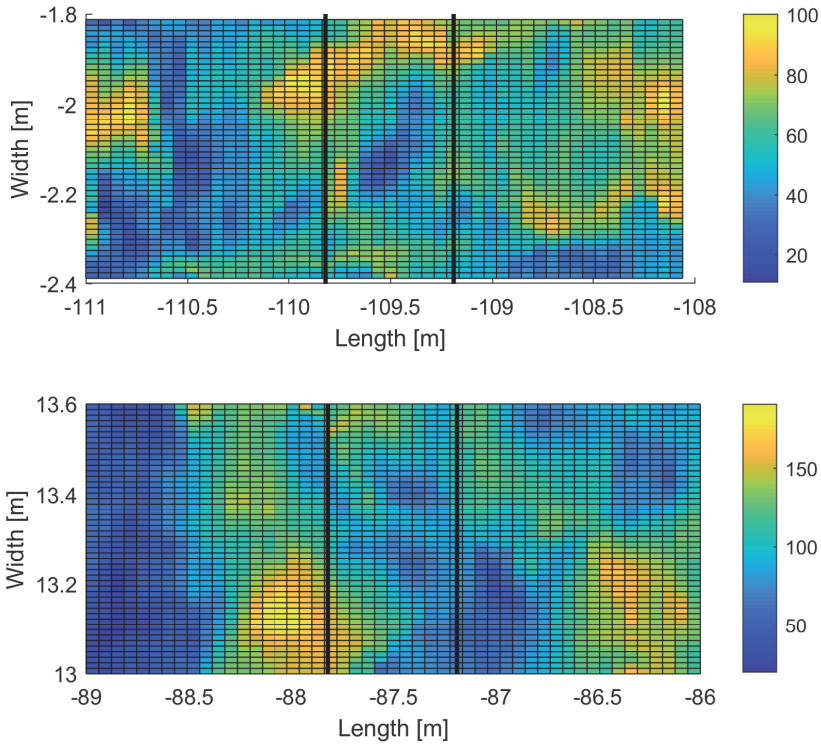

Figure 4.14: Contour plot that shows the variation in shotcrete thickness for two of the studied cases. Length and width are plotted in global coordinates and the thickness is expressed in mm. Solid lines indicate location of the rock joints. From Sjölander et al. [106].

interface and bending of the shotcrete. Due to this, an increased joint-distance increases the lever arm for the force, which affects the structural capacity and behaviour of the lining. The effect of the joint-distance is shown to the right in Figure 4.15. With an increased joint distance, the stresses due to bending increase, which reduce the maximum force the lining can carry.

Similar to the study with respect to bond strength, the variations in shotcrete thickness h_{s} in the area enclosed by the width of the slab and the length subjected to tensile bond stress, δ_{b} was studied. Based on the ten cases studied, the correlations between $F_{\max}$ and $h_{\mathrm{s,min}}$, $h_{\mathrm{s,mean}}$ and $h_{\mathrm{s,max}}$ are shown in Figure 4.16. As for the bond strength, a strong linear correlation exist between $F_{\max}$ and the mean shotcrete thickness $h_{\mathrm{s,mean}}$.

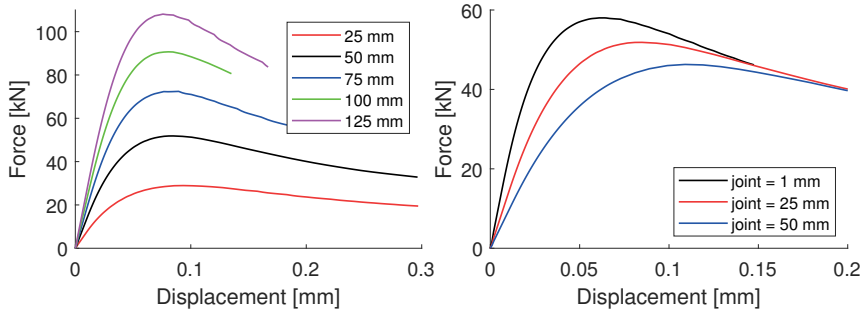

Figure 4.15: The left figure shows the relationship between force and vertical displacement of the centric block for the cases with uniform thickness. The right figure shows how the joint distance between the blocks affects the structural capacity for a case with a uniform thickness of 50 mm. From Sjölander et al. [106].

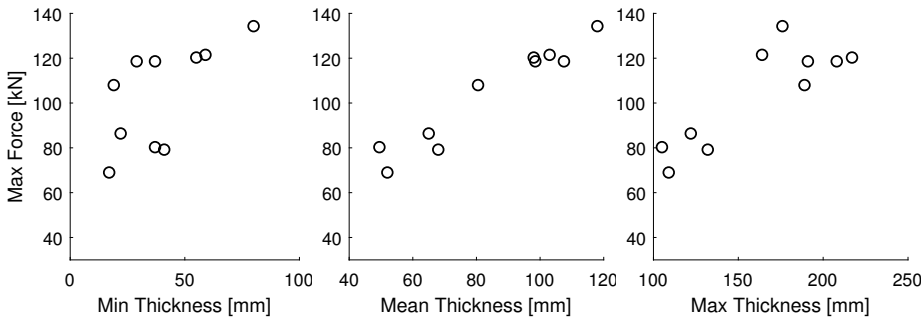

Figure 4.16: Correlation between maximum force and minimum, mean and maximum shotcrete thickness in the area subjected to tensile bond stress. From Sjölander et al. [106].

Table 4.5: Results from the case study on structural capacity of shotcrete linings with varying thickness. From Sjölander et al. [106].

Case	$F_{\max}$ **[kN]**	$h_{\mathrm{s,mean}}$ **[mm]**	$h_{\mathrm{s,min}}$ **[mm]**	$h_{\mathrm{s,max}}$ **[mm]**	F_{uni} **[kN]**	$F_{\max}/F_{\mathrm{uni}}$ **[-]**
1	79	68	41	132	75	1.05
2	119	99	29	208	104	1.14
3	122	103	59	164	106	1.15
4	119	108	37	191	104	1.14
5	69	52	17	109	67	1.03
6	108	81	19	189	96	1.13
7	134	118	80	176	115	1.17
8	120	98	55	217	105	1.14
9	86	65	22	122	81	1.06
10	80	50	37	105	76	1.05

A more detailed comparison of the effects of varying thickness with respect to the structural capacity is presented in Table 4.5. Here, $F_{\max}$ is presented for each of the ten studied cases with varying shotcrete thickness. Furthermore, the mean $h_{\mathrm{s,mean}}$, minimum $h_{\mathrm{s,min}}$ and maximum $h_{\mathrm{s,max}}$ shotcrete thickness in the area subjected to tensile bond stresses are presented. Finally, the structural capacity for the shotcrete was estimated based on the mean thickness, F_{uni}. This was calculated based on linear inter- and extrapolation from the simulations with uniform thickness presented to the left in Figure 4.15. The results in Table 4.5 indicate that local variations in shotcrete thickness can be large in comparison to the mean value without having any significant effect on the structural capacity. This can be seen by comparing Cases 2 to 4 which have similar $h_{\mathrm{s,mean}}$ and $F_{\max}$, while the relative variability in $h_{\mathrm{s,min}}$ and $h_{\mathrm{s,max}}$ is large. Moreover, for Case 5, 6 and 9 $h_{\mathrm{s,min}}$ is similar but large differences can be seen in $F_{\max}$. This means that the minimum thickness has if any, a minor influence on the structural capacity. For these cases, $F_{\max}$ is increased with an increased $h_{\mathrm{s,mean}}$. In the last column of Table 4.5, the ratio between $F_{\max}$ and F_{uni} is presented. This shows that $F_{\max}$ is between 3 and 17% higher than F_{uni}, which indicates that the maximum thickness has some influence on the structural capacity. Furthermore, this means that a design based on the mean value of thickness is conservative.

4.3.3 Failure mechanism of a bolt-anchored lining

The failure of a bolt-anchored and FRS lining is complex and involves many possible failure mechanisms, such as; cracking of FRS, bond failure between shotcrete and rock, tensile failure of rock bolts and failure along the bolt-grout or grout-rock interfaces. The failure of this system has been studied experimentally by Fernandez-Delgado et al. [42] and by Holmgren [56; 58]. In a paper by Sjölander et al. [104], the individual failure mechanisms for a bolt anchored FRS lining were analysed, and numerical models for each of the failures were presented and verified individually. In [105], the model was refined and used to study the failure mechanisms for the complete system. This includes cracking of shotcrete, bond failure between shotcrete and rock, pull-out failure of rock bolts and yielding of rock bolts. Experimental results from Holmgren [58] were used as reference. The numerical model is here schematically shown in Figure 4.17.

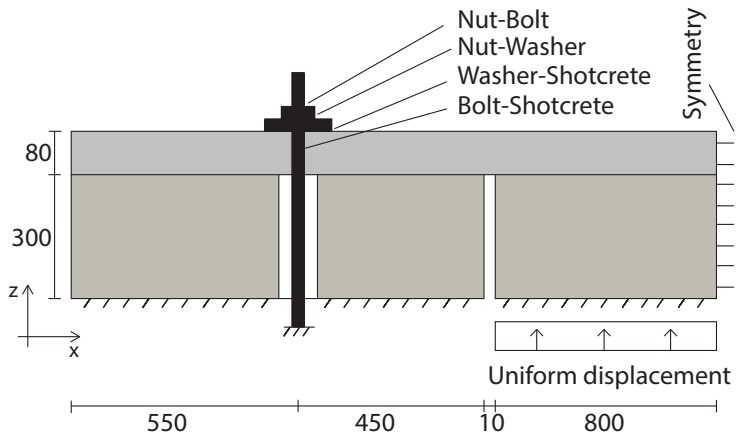

Figure 4.17: Numerical model used by Sjölander et al. [105] for a bolt-anchored and FRS lining. Dimensions are given in mm.

First, the numerical model was used to verify the structural behaviour of the experiments from Holmgren [58]. The width of the specimen was reduced from 1200 to 800 mm to decrease the computational time. To be able to compare results from simulations and experiments, all results were normalized to their maximum value as presented in Figure 4.18. After reaching the peak-load, the force is reduced to an approximate level of 40% in both the experiments and the simulations. The circle markers indicate data points from the experiments, which shows that the softening part was not captured. Thereafter, some hardening can be seen in the experiments, while the force was kept constant in the simulations. This could indicate that the horizontal boundary conditions for the experiments were not entirely captured in the model. In order for a crack to propagate, a displacement must occur in the x-direction, see Figure 4.17. The boundary condition in the x-direction was modelled with a spring and it is possible that this does not fully capture the boundary conditions from the experiment. The hardening could also be caused by the fibres. A scatter in the post-cracking response is always seen during testing of fibre-reinforced shotcrete, due to the natural variation in number and orientation of the fibres that bridge the crack. Since the model parameters were chosen based on fitting experimental results for one beam, it is natural that the structural response was not captured perfectly. It is also possible that the hardening effects was caused by hardening of the steel, which was modelled as elastic-perfectly plastic and thus, neglected any effect of local hardening. However, the results show a good agreement between the simulated and experimental results, which means that the numerical model was able to capture the structural behaviour.

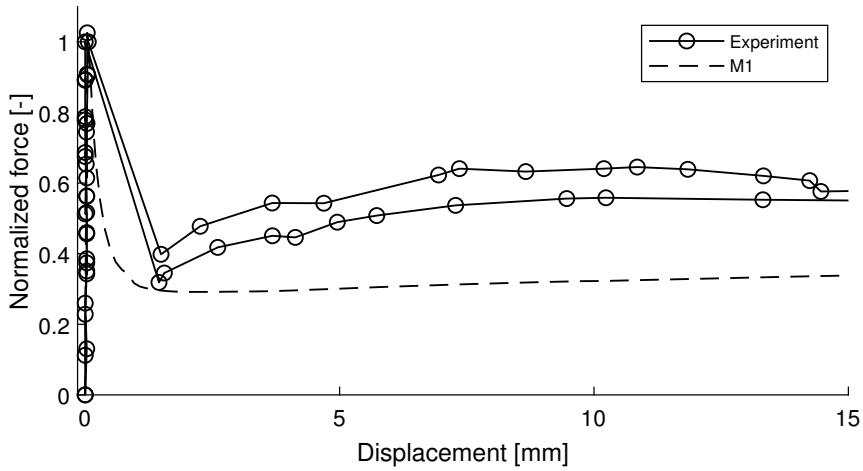

Figure 4.18: Relationship between force and vertical displacement of the centric block for numerical simulations and experimental results from Holmgren [58]. Results have been normalized to their respective maximum value. From Sjölander et al. [105].

Then, the numerical model was used to study how each of the failure mechanism contributes to the structural behaviour. This was done by comparing five models, M1 to M5. In the first model (M1), all failure mechanisms were considered, i.e. cracking of fibre-reinforced shotcrete, bond failure between shotcrete and rock, pull-out failure and yielding of rock bolts. For the other models, M2 to M5, changes were made accordingly:

- **M2:** No bond between the outer block (left block in Figure 4.17) and shotcrete. Full bond exists between the moving block and shotcrete.
- **M3:** Shotcrete was modelled as linear elastic.
- **M4:** The rock bolt was moved and placed 650 mm from the joint between the blocks, instead of 450 mm.
- **M5:** Shotcrete was modelled as unreinforced.

The influence of each failure mode is shown in Figure 4.19 which has been divided into three different phases, (I to III), to describe how the studied failure mechanisms affect the structural behaviour. The initial stiff response of the lining during phase I is due to the bond between shotcrete and rock. This is made clear by comparing the response for M2, in which no bond exists between the outer block and shotcrete, to that of all other models. For M2, the initial response is governed by the elastic stiffness of the shotcrete. The first peak load for M2 is determined by the tensile strength of the shotcrete. For the other cases, the first

peak load was determined by the bond strength. After reaching the peak load, a softening response is seen, which is the start of phase II. During this phase the force is continuously decreasing while the bond failure propagates and cracks start to form in the shotcrete. When the bond failure has propagated to the location of the rock bolt, it is arrested, which is the end of phase II. In phase III, the load from the moving block will be transferred to the rock bolt through bending of the shotcrete and the washer plate. Cracks in the shotcrete, close to the joint between the moving block and rock bolt, start to increase in width and propagate further through the shotcrete thickness. The structural response at the beginning of phase III is governed by the residual strength and stiffness of the FRS. It can be noted that for M3, no cracks forms and the structural response is therefore governed by the elastic stiffness of the shotcrete. By comparing the results from M1 to M3, it is clear that M3 represents the upper limit for the shotcrete stiffness. Depending on the type and amount of fibres used as well as the bond strength, the residual capacity of the lining might be higher than the initial peak load caused by bond failure. The ultimate failure of the lining, which was not studied here, then occurs when either the rock bolt fails due to pull-out or rupture, or the FRS fails due to extensive cracking.

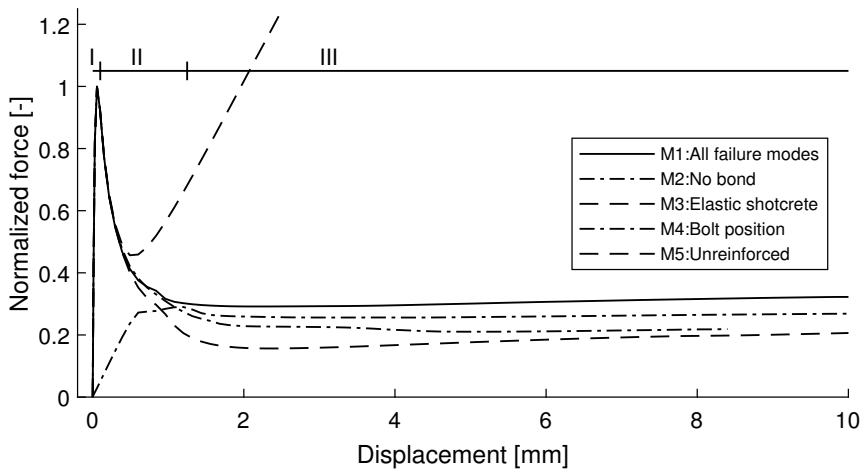

Figure 4.19: Relationship between force and vertical displacement of the centric block for model M1 to M5. From Sjölander et al. [105].

Chapter 5

Discussion

In this chapter, a general discussion of the work and results from this report is presented. A more detailed discussion regarding the different topics covered by this report are presented by Bjureland et al. [16], Sjölander and Ansell [101; 102] and Sjölander et al. [105; 106].

5.1 General discussion

Tunnels in a hard and jointed rock mass are complex structures, and many uncertainties exist during the design, construction and assessment of such structures. The numerical design of a tunnel is often performed using deterministic and uniform values for shotcrete thickness and bond strength. As shown by e.g. Malmgren et al. [78], Ansell [5] and Bjureland et al. [16], large variations in shotcrete thickness and bond strength should be expected. How local variations in thickness and strength affect the structural behaviour and capacity for a shotcrete lining is not completely understood and was the main focus on this doctoral project.

In order to succeed with this, in-situ data of shotcrete thickness and mechanical parameters were collected to quantify the variations. Numerical simulations were performed to investigate how such variations affect the structural behaviour and cracking of the shotcrete. For this purpose, well-defined load cases represented by drying shrinkage and the gravity load from a loose block were used. Models for fibre reinforced concrete and shotcrete [87; 108; 124] and rock bolts [34; 66; 110] are well studied, while few papers are devoted to modelling of bond failure between shotcrete and rock, see e.g. Dong et al. [37; 38; 39]. The main contribution of this report, with respect to modelling, is the numerical model suitable for the structural analyses of fibre-reinforced shotcrete (FRS) in interaction with hard rock, rock bolts and steel plates. The numerical models for FRS and bond has throughout the work with this report been gradually refined. For FRS, a softening function was developed inspired by the tri-linear softening model presented by Yoo et al. [124], and composite models presented by e.g. Soetens and Matthys [108] and Bernardi et al. [14]. This softening function is presented

in Section 3.2 and was first published by Sjölander et al. [104]. Furthermore, since only a few papers have focused on the numerical modelling for bond failure between shotcrete and rock, the model and suggested material properties of the interface in this report have provided a tool to investigate the bond failure.

The numerical model presented in this report was used to investigate the structural behaviour and cracking of shotcrete when subjected to shrinkage or the load from a loose block. In most experimental set-ups, a uniform shotcrete thickness has been used, either through casting or by levelling of the surface directly after spraying. Few experiments exist in which sprayed shotcrete with varying thickness are used, and if so, the variations are seldom reported. Therefore, experiments with uniform thickness were used to verify the structural behaviour of the numerical model. Then, variations in shotcrete thickness have been applied to study how this affects the behaviour.

5.2 In-situ variations of shotcrete thickness and bond strength

Many uncertainties exist in the design of a rock tunnel. The quality of the rock is estimated based on in-situ testing, empirical knowledge and engineering judgement. Based on this, the rock support is typically designed based on a combination of empirical knowledge and numerical modelling, which yield a required shotcrete thickness and bond strength. A test program for the rock support is set-up and return results during the tunnel construction. Data collected within a control program for the construction of a railway tunnel in Stockholm, Sweden were used to propose distributions of shotcrete strength, thickness and bond strength. These data were presented by Bjureland et al. [16] and showed that the mean value of the applied thickness was 25 mm more than the required thickness. This was regardless if the required thickness was 50, 75 or 100 mm. However, the coefficient of variation was more than 30% which indicates that the required thickness was not achieved in many sections. Estimating the shotcrete thickness during spraying is difficult. No clear visual markers exist, and the visibility is limited during spraying. To ensure that a sufficient thickness is sprayed, the operator might spray extra shotcrete. Besides the increased risk of failure, the operator must go back to spray additional shotcrete if the requirements for thickness are not met. This could cause a delay in the construction, and for this reason, it might be more feasible for the contractor to spray more shotcrete the first time. Today, laser scanners mounted on the spray robot, see Section 2.3, can be used to measure the actual shotcrete thickness directly after spraying. This way, the operator gets immediate feedback on the thickness and can apply more shotcrete in the required sections. This immediate feedback eliminates the risk of not reaching the required thickness and gives a better control of the applied thickness. This could reduce the large variability in shotcrete and has a great potential of saving money and decreasing the

environmental impact of the tunnel.

In [16], a normal distribution with the mean value and standard deviation of 0.81 and 0.32 MPa, respectively, was found to describe the data accurately. The data consisted of 354 discrete samples, and the large variability in bond strength corresponds with results presented by e.g. Malmgren [78]. As discussed in Section 2.4, the development of bond strength depends on many factors, and variations should therefore be expected. The requirements for the studied project was that the mean value for a test series with three test samples should exceed 0.5 MPa. This means that the probability that a single value is higher than the required values is approximately 68%. Furthermore, it was shown that when failures occur at a stress equal to, or less than 0.5 MPa, 50% or more of the failure surface was in the rock mass, see Figure 4.2. This means that if loose small rock fragments could be removed before spraying, by e.g. hydro-scaling, the quality of the bond could likely be improved.

The data presented by Bjureland et al. [16] were collected from one project, and the suggested distributions could, to some extent, depend on factors related to the project and site, such as the contractor who performs the work, the supplier of the shotcrete, and of course the properties of the rock. To better understand how such factors affect the distributions, data should be collected from more projects in future studies. Due to these uncertainties, the presented distributions might not be representative for other tunnels. The presented data should therefore not be used in the design of a new tunnel.

5.3 Structural behaviour of a shotcrete lining

Numerical simulations of cracking induced by drying shrinkage for a continuously restrained and end-restrained shotcrete slab were presented by Sjölander and Ansell [101; 102]. The results from these papers have shown that the variations in shotcrete thickness will not have any significant effects on the structural behaviour when shotcrete is subjected to shrinkage. Cracks will preferably form in locally weak parts, i.e. in sections with low thickness or abrupt changes in thickness. Fibre-reinforced shotcrete has often a strain-softening behaviour. This means that, preferably, one wide crack forms in shotcrete instead of several narrow cracks. Experimental results from Malmgren and Nordlund [77] and Carlswärd [26], as well as results from Sjölander and Ansell [101], show that multiple cracks form in shotcrete subjected to shrinkage with a continuous bond to a stiff substrate, i.e. concrete or rock. This is similar to the structural behaviour of reinforced shotcrete. In this case, the substrate acts as reinforcement, and it was shown by Groth [48] that the width of the crack increases with an increased thickness of the overlay, i.e. here the shotcrete thickness. Therefore, in terms of cracking, it is more beneficial to have a uniform or close to uniform shotcrete thickness and sections with

excessive thickness should be avoided. With a more uniform thickness, drying will be more uniform, which reduces local restraint caused by moisture gradients over the shotcrete surface.

In the paper by Sjölander et al. [106], numerical simulations were performed to investigate how the structural capacity for bonded shotcrete lining was affected by local variations in shotcrete thickness and bond strength. Today, it is uncertain how and if the shotcrete thickness affects the structural capacity of the lining. Stille [112], suggests a linear relationship between the structural capacity and shotcrete thickness, while Barrett and McCreath [10] neglects the shotcrete thickness in their calculation of the structural capacity. In the numerical simulations, a strong linear correlation was found between the mean value of the thickness in the area subjected to tensile bond stress and the structural capacity. The same was true for the variations in bond strength, in which a strong linear correlation exists between the mean value of the bond strength and the structural capacity. This seems reasonable since bond failure occurs at small displacements, and both the concrete and the interface are stiff. This combination will enforce that the bond failure will propagate and increase uniformly along each side of the block. This is true as long as local areas with low thickness or bond strength are sufficiently small to be balanced by local areas with higher thickness or bond strength. It should be stressed that the size and distribution of the local weak areas were not studied in detail. This is an important aspect for future studies.

In the design of a shotcrete lining, individual failure modes suggested by Barrett and McCreath [10] are commonly used. Based on these, shotcrete fails either due to bond, flexural or shear failure. These failure modes have been derived from experimental testing [42; 56; 58]. In Sjölander et al. [105], a numerical model capable of simulating the failure of a bolt-anchored and fibre-reinforced shotcrete lining was presented. The model showed good agreement with results from large-scale testing [58] and provides an important tool that can be used in future studies on the structural behaviour of shotcrete. The presented results confirmed that the failure mechanisms of the lining can be treated individually in the design as suggested by Barrett and McCreath [10]. One important aspect for future studies is to include conditions such as the in-situ stress in the rock mass, variations in shotcrete thickness and the shape of the tunnel roof. This will result in an initial state of stress in the shotcrete which could affect the structural behaviour and failure mode that develops.

Chapter 6

Conclusions and further research

In this chapter, the conclusions from this report are presented. Then, two research projects that have been initiated in connection to this doctoral project are presented, followed by some suggestions for further research.

6.1 Conclusions

In this report, numerical simulations have been used to simulate the structural behaviour of fibre-reinforced shotcrete in interaction with hard rock and rock bolts. The focus of the presented work was to understand how variations in shotcrete thickness and bond strength affect the cracking and structural capacity for a shotcrete lining. This is of importance since previous research, and collected field data show large variations in these parameters. Below, the conclusion from this report are presented.

It is known that variations in shotcrete thickness and bond exist in-situ and that these parameters are crucial for the capacity of the shotcrete lining. In the work by Bjureland et al. [16], the aim was to quantify the variations in these parameters and highlight how such variations could be used for a reliability-based verification of the rock support capacity. Based on more than 6000 measurements of thickness and 350 tests of bond strength, the variations in shotcrete thickness and bond strength can be described with a log-normal and normal distribution, respectively. Moreover, the data presented in [16] showed that the required strength and thickness for the studied project, normally, were fulfilled. However, local areas with low bond strength and thickness will exist. Any possible correlation between these parameters were not studied. Furthermore, there was a clear tendency of spraying too much shotcrete and the mean thickness was approximately 25 mm higher compared to the required thickness. For the bond strength, the results indicated that no correlation exists between the bond strength and the estimated RMR-value for granite or gneiss. This means that even though the quality of the rock could be decisive for the bond strength, the RMR-value should no be used as the only indication to determine whether or not a sufficient bond strength could be achieved.

When shotcrete is subjected to shrinkage, the results presented by Sjölander and Ansell [101] showed that wide cracks form in areas where the shotcrete has partly lost bond. Therefore, wide cracks in the shotcrete is a good indication of local bond failure. The reason to the formation of wide cracks is that the fibre-reinforced shotcrete normally has a strain-softening behaviour. This means that the load cannot be increased after the first crack forms. However, a pattern of fine and narrow cracks forms when the shotcrete has a continuous bond to the rock. In that case, the rock acts as reinforcement for the shotcrete. This effect decreases with an increased shotcrete thickness, which means that sections with excessive thickness should be avoided.

Numerical simulations showed that when unreinforced shotcrete with varying thickness is subjected to shrinkage, several fine and narrow cracks form if the bond to the rock is continuous. In such case, the variations in shotcrete thickness do not have any significant effect on the number, or width of the cracks. The localisation of cracks was governed by sections with low stiffness, or abrupt changes in thickness. Since the rate of drying is greatly affected by the thickness of the shotcrete, large variations in thickness could lead to an increased local restraint in the shotcrete caused by the gradients in drying.

Previous studies have, as fas as the author knows, not been conducted to investigate how the structural capacity of a shotcrete lining, with respect to bond failure, is affected by local variations in shotcrete thickness and bond strength. Therefore, the effects of both uniform and local variations in shotcrete thickness and bond strength were studied by Sjölander et al. [106]. In contradiction to experimental results and design models, the results indicate that the shotcrete thickness has a significant effect on the structural capacity for the lining with respect to bond failure. For local variations, the simulations indicate that there is a strong linear correlation between the mean value of the thickness and the bond strength around a narrow perimeter, 50 to 200 mm, of the block. Moreover, local areas with low thickness and bond strength could exist around the perimeter without having a significant effect on the structural capacity. However, it was also concluded that the magnitude of these weak areas, and their mutual placement around the perimeter, are important parameters that were not included in this study.

A bolt-anchored and fibre reinforced shotcrete lining is normally designed based on analytical solutions that assume individual failure modes, e.g. cracking of shotcrete or bond failure. This design model has been derived from experimental testing. A numerical model capable of simulating the complex failure of a bolt-anchored lining was presented and showed good agreement with full-scale experimental testing. The simulated results confirm that failure mechanism can be treated individually which is the basic assumption for the derived analytical solutions commonly used in the design of a shotcrete lining. The design of a shotcrete lining should therefore be based on individual failure modes. Moreover, it was shown that a conservative design of the lining should be based on the residual strength of the shotcrete. However, the structural capacity with respect to bond

failure could yield a more economic design. More research is needed in order to understand how the variations in bond strength presented in [16] should be treated in order to yield a safe design.

6.2 Initiated research projects

As a result of the work presented in this doctoral project, two research projects have been initiated and are briefly described below.

TACK - Tunnel Automatic CracK Detection
This project aims to create an autonomous inspection method for tunnels. Today, the inspections of tunnels are mainly performed by ocular inspections, which is time-consuming and prone to human errors. According to Lindblom [73], this strategy makes it impossible to inspect the whole tunnel. This is due to the limited time available for inspections since the tunnel must be closed for traffic during the inspection. Today, mobile mapping systems equipped with geomatic sensors such as laser scanners, optic and infrared cameras can capture and collect data to reconstruct a 3D model of the tunnel. Today, these data are then inspected to detect cracks or other defects on the shotcrete surface.

In this project, a hybrid approach with machine learning and photogrammetry will be used to automatically detect and measure the propagation of cracks from imagery acquired with a mobile mapping system [107]. Then, the collected geometric features of the cracks should be used to evaluate the risk associated with the cracks. The project is funded by The Swedish Transport Administration and Vinnova through the call InfraSweden 2030.

Use of alternative fibres in Swedish traffic tunnels
In Sweden, there is a strong tradition of using steel-fibres as reinforcement for permanent shotcrete linings and today, fibres made of alternative materials, e.g. basalt or synthetic, are not allowed by the Swedish Transport Administration to be used in Swedish road and railway tunnels. The main reason for this is that the long-term structural behaviour and deterioration mechanisms for steel fibres are well known. For alternative fibres, the structural behaviour is normally well tested by manufacturers and researcher, but the long-term behaviour and durability, especially when the technical life-span is 120 year is uncertain.

This research project is initiated and funded by the Swedish Transport Administration, and the aim is to investigate if alternative fibres are suitable to use in Swedish road and railway tunnels. The project does not only consider the structural behaviour and durability for the fibres, but also the environmental impact of different fibres will be evaluated.

6.3 Suggestions for further research

Finally, based on the work presented in this report, some interesting topics for further research have been identified and are presented below.

Experimental testing should be performed to confirm, or reject, the results presented in [106] which showed that the shotcrete thickness affects the structural capacity with respect to bond failure when the lining is subjected to a block load. If the shotcrete thickness affects the structural capacity, some new design recommendations should be developed that consider this.

Numerical simulations should be performed to understand how the size of local areas with a low bond strength and their mutual placement around the perimeter of the block affect the structural capacity when the lining is subjected to a block load. In combination with this, in-situ or laboratory data should be collected to better understand the spatial correlation of the bond strength.

The structural behaviour and failure modes for a bolt-anchored shotcrete lining should be investigated with boundary conditions similar to the in-situ situation, i.e. considering horizontal in-situ stresses in the rock mass and variations in geometry.

Today, LiDAR scanning is used in many projects to scan the rock and the shotcrete surface. This is an excellent source of data that could be used to study the in-situ variations in shotcrete thickness in detail. With this type of data we could better understand to what extent the variations in thickness depends on factors such as the operator and deviations in tunnel shape.

For the assessment of tunnels, it should be investigated how pre-existing cracks affect the structural behaviour and capacity of the shotcrete. To what level do the geometric features, direction and location of the cracks affect the structural capacity and what type of cracks should be considered as potentially dangerous for the safety of the tunnel.

During excavation with the drill and blast method, underbreak and overbreak occur due to variations in the rock mass properties. This forms local pits and spikes which could affect the structural behaviour of the shotcrete lining when subjected to shrinkage, e.g. the risk of debonding might increase around a local pit.

Bibliography

[1] Abaqus. *Abaqus ver. 6.14 Documentation*. Providence, USA, 2014.

[2] L. Ahmed. *Models for analysis of young cast and sprayed concrete subjected to impact-type loads*. Ph.D Thesis. KTH Royal Institute of Technology. Stockholm, Sweden, 2015.

[3] M.G. Alexander, S. Mindess, S. Diamond, and L. Qu. Properties of paste-rock interfaces and their influence on composite behaviour. *Materials and Structures*, 28(9):497–506, 1995. doi: 10.1007/BF02473154.

[4] A. Ansell. *Dynamically loaded rock reinforcement*. Ph.D Thesis. KTH Royal Institute of Technology. Stockholm, Sweden, 1999.

[5] A. Ansell. Investigation of shrinkage cracking in shotcrete on tunnel drains. *Tunnelling and Underground Space Technology*, 25:607–613, 2010. doi: 10.1016/j.tust.2010.04.006.

[6] S. Austin and P. Robins. *Sprayed concrete: Properties, design and application*. Whittles Publishing, Latheronwheel, UK, 1995. ISBN 187032501X.

[7] S. Austin, P. Robins, and Y. Pan. Tensile bond testing of concrete repairs. *Materials and Structures*, 28(5):249–259, 1995. doi: 10.1007/BF02473259.

[8] N. Banthia. Steel fibre-reinforced concrete at sub-zero temperatures: From micromechanics to macromechanics. *Journal of Materials Science Letters*, 11:1219–1222, 1992. doi: 10.1007/BF00729773.

[9] N. Banthia, M. Azzabi, and M. Pigeon. Restrained shrinkage cracking in fibre-reinforced cementitious composites. *Materials and Structures*, 26(7):405–413, 1993. doi: 10.1007/BF02472941.

[10] S.V.L. Barrett and D.R. McCreath. Shortcrete support design in blocky ground: Towards a deterministic approach. *Tunnelling and Underground Space Technology*, 10(1):79–89, 1995. doi: 10.1016/0886-7798(94)00067-U.

[11] N. Barton, R. Lien, and J. Lunde. Engineering classification of rock masses for the design of tunnel support. *Rock Mechanics*, (6):189–236, 1974. doi: 10.1007/BF01239496.

[12] Z.P. Bažant and L.J. Najjar. Nonlinear water diffusion in nonsaturated concrete. *Matriaux et Constructions*, 5(1):3–20, 1972. doi: 10.1007/BF02479073.

[13] Z.P. Bažant and B.H. Oh. Crack band theory for fracture of concrete. *Matériaux et construction*, 16(3):155–177, 1983. doi: 10.1007/BF02486267.

[14] P. Bernardi, R. Cerioni, and E. Michelini. Analysis of post-cracking stage in SFRC elements through a non-linear numerical approach. *Engineering Fracture Mechanics*, 108:238–250, 2013. doi: 10.1016/j.engfracmech.2013.02.024.

[15] Z.T. Bieniawski. Engineering classification of jointed rock masses. *Civil Engineer in South Africa*, 15(12), 1973. doi: 10.1016/0148-9062(74)90924-3.

[16] W. Bjureland, Johansson F., A. Sjölander, J Spross, and S. Larsson. Probability distributions of shotcrete parameters for reliability-based analyses of rock tunnel support. *Tunnelling and Underground Space Technology*, 87:15–26, 2019. doi: 10.1016/j.tust.2019.02.002.

[17] L. Blanco Martín, M. Tijani, F. Hadj-Hassen, and A. Noiret. Assessment of the bolt-grout interface behaviour of fully grouted rockbolts from laboratory experiments under axial loads. *International Journal of Rock Mechanics and Mining Sciences*, 63:50–61, 2013. doi: 10.1016/j.ijrmms.2013.06.007.

[18] T. Brady, L. Martin, and R. Pakalnis. Empirical approaches for opening design in weak rock masses. *Mining Technology*, 114(1), 2005. doi: 10.1179/037178405X44494.

[19] T. L. Brekke, H. H. Einstein, and R. E. Mason. *State-of-the-art review on shotcrete*. Final report, U.S Army Engineer Waterways Experiment Station, Virgina, USA, 1976.

[20] L.E. Bryne. *Time dependent material properties of shotcrete for hard rock tunneling*. Ph.D Thesis. KTH Royal Institute of Technology. Stockholm, Sweden, 2014.

[21] L.E. Bryne, A. Ansell, and J. Holmgren. Laboratory testing of early age bond strength of shotcrete on hard rock. *Tunnelling and Underground Space Technology*, 41:113–119, 2014. doi: 10.1016/j.tust.2013.12.002.

[22] L.E. Bryne, A. Ansell, and J. Holmgren. Investigation of restrained shrinkage cracking in partially fixed shotcrete linings. *Tunnelling and Underground Space Technology*, 42:136–143, 2014. doi: 10.1016/j.tust.2014.02.011.

[23] L.E. Bryne, J. Holmgren, and A. Ansell. Shrinkage testing of end-restrained shotcrete on granite slabs. *Magazine of Concrete Research*, pages 1–11, 2014. doi: 10.1680/macr.13.00348.

[24] N. Buratti, C. Mazzotti, and M. Savoia. Post-cracking behaviour of steel and macro-synthetic fibre-reinforced concretes. *Construction and Building Materials*, 25(5):2713–2722, 2011. doi: 10.1016/j.conbuildmat.2010.12.022.

[25] P. Camanho and C.G. Davila. Mixed-mode decohesion finite elements in for the simulation composite of delamination materials. *Nasa*, TM-2002-21: 1–37, 2002. doi: 10.1177/002199803034505.

[26] J. Carlswärd. *Shrinkage cracking of steel fibre reinforced self compacting concrete overlays Test methods and theoretical modelling*. Ph.D Thesis. Luleå University of Technology. Luleå, Sweden, 2006.

[27] CEN. *Eurocode: Basis of structural design*. Technical report, European Committee for Standardisation, Brussels, Belgium, 2004.

[28] CEN. *Eurocode 2: Design of concrete structure -Part 1-1 General rules and rules for buildings*. Technical report, European Committee for Standardisation, Brussels, Belgium, 2004.

[29] CEN. *Eurocode 7: Geotechnical design -Part 1 General rules*. Technical report, Brussels, Belgium, 2004.

[30] CEN. *EN 14488-3: Testing sprayed concrete - Part 3: Flexural strengths (first peak, ultimate and residual) of fibre reinforced beam specimens*. Technical report, European Committee for Standardisation, Brussels, Belgium, 2006.

[31] CEN. *EN 14488-6: Testing sprayed concrete Part 6: Thickness of concrete on a substrate*. Technical report, European Committee for Standardisation, Brussels, Belgium, 2006.

[32] CEN. *EN 14488-4: Testing sprayed concrete - Part 4: Bond strength of cores by direct tension*. Technical report, European Committee for Standardisation, Brussels, Belgium, 2008.

[33] CEN. *EN 12504-1: Testing concrete in structures - Part 1: Cored specimens - Taking, examining and testing in compression*. Technical report, European Committee for Standardisation, Brussels, Belgium, 2009.

[34] S.H. Chen, S. Qiang, S.F. Chen, and P. Egger. Composite element model of the fully grouted rock bolt. *Rock Mech. Rock Engng*, 37(3):193–212, 2004. doi: 10.1007/s00603-003-0006-z.

[35] Comsol. *Comsol Multiphysics ver. 5.4 Documentation*. Stockholm, Sweden, 2019.

[36] R.D. Cook, D.S. Malkus, M.E. Plesha, and R.J. Witt. *Concepts and applications of finite element analysis*. John Wiley and Sons, Inc., New York, USA, fourth edition, 2002. ISBN 0471356050.

[37] W. Dong, Z. Wu, and X. Zhou. Fracture mechanisms of rock-concrete interface : Experimental and numerical. 142(7):1–11, 2016. doi: 10.1061/(ASCE)EM.1943-7889.0001099.

[38] W. Dong, Z. Wu, X. Zhou, N. Wang, and G. Kastiukas. An experimental study on crack propagation at rock-concrete interface using digital image correlation technique. *Engineering Fracture Mechanics*, 171:50–63, 2017. doi: 10.1016/j.engfracmech.2016.12.003.

[39] W. Dong, D. Yang, X. Zhou, G. Kastiukas, and B. Zhang. Experimental and numerical investigations on fracture process zone of rock-concrete interface. *Fatigue and Fracture of Engineering Materials and Structures*, 40(5): 820–835, 2017. doi: 10.1111/ffe.12558.

[40] N. El-Zain. *An experimental study of the validity of the round panel test method for shotcrete*. Master Thesis. KTH Royal Institute of Technology. Stockholm, Sweden, 2018.

[41] S. Fekete, M. Diederichs, and M. Lato. Geotechnical and operational applications for 3-dimensional laser scanning in drill and blast tunnels. *Tunnelling and Underground Space Technology*, 25(5):614–628, 2010. doi: 10.1016/j.tust.2010.04.008.

[42] G. Fernandez-Delgado, J. Mahar, and E. Cording. *Shotcrete: Structural testing of thin liners*. Technical report, University of Illinois, Washington, USA, 1975.

[43] T. Franzén. Shotcrete for underground support: a state-of-the-art report with focus on steel-fibre reinforcement. *Tunnelling and Underground Space Technology*, 7(4):383–391, 1992. doi: 10.1016/0886-7798(92)90068-S.

[44] A. Fredriksson, J. Johansson, L. Persson, and B. Stille. *Drains for rock tunnels - Function and design*. Technical report, Stockholm, Sweden, 1996.

[45] T. Gasch. *Concrete as a multi-physical material with applications to hydro power facilities*. Licentiate Thesis. KTH Royal Institute of Technology. Stockholm, Sweden, 2016.

[46] T. Gasch. *Multiphysical analysis methods to predict the ageing and durability of concrete*. Ph.D Thesis. KTH Royal Institute of Technology. Stockholm, Sweden, 2019.

[47] T. Gasch, R. Malm, and A. Ansell. A coupled hygro-thermo-mechanical model for concrete subjected to variable environmental conditions. *International Journal of Solids and Structures*, 91:143–156, 2016. doi: 10.1016/j.ijsolstr.2016.03.004.

[48] P. Groth. *Fibre reinforced concrete*. Ph.D Thesis. Luleå University of Technology. Luleå, Sweden, 2010.

[49] T. Hahn. *Adhesion of shotcrete to various types of rock surfaces*. Report 55, Rock Engineering Research Foundation, Stockholm, Sweden, 1983.

[50] A.L. Hammer, M. Thewes, and R. Galler. Empirical forecasting model to determine the strength development of shotcrete. *Geomechanik und Tunnelbau*, 12(6):730–738, 2019. doi: 10.1002/geot.201900054.

[51] M.A.N. Hendriks, A. de Boer, and B. Belletti. *Guidelines nonlinear finite element analysis of concrete structures*. Document rtd 1016:2012„ Ministry of Infrastructure and Environment, the Netherlands, 2017.

[52] A. Hillerborg, M. Modéer, and P.-E. Petersson. Analysis of crack formation and crack growth in concrete by means of fracture mechanics and finite elements. *Cement and Concrete Research*, 6(6):773–781, 1976. doi: 10.1016/0008-8846(76)90007-7.

[53] E. Hoek and Brown E.T. *Underground excavations in rock*. Institution of Mining and Metallurgy, London, UK, 1980. ISBN 0900488549.

[54] E. Hoek, P.K. Kaiser, and W.F. Bawden. *Design of support for underground hard rock mines*. Mining Research Directorate and Universities Research Incentive Fund, Toronto, Canada, 1993.

[55] E. Hoek, P.K. Kaiser, and W.F. Bawden. *Support of underground excavations in hard rock*. A. A. Balkema, Rotterdam, the Netherlands, 2000.

[56] J. Holmgren. *Punch-loaded shotcrete linings on hard rock*. Technical report, Rock Engineering Research Foundation, Stockholm, Sweden, 1979.

[57] J. Holmgren. *Dynamically loaded rock reinforcement of shotcrete*. Technical report, Swedish Fortification Agency, Stockholm, Sweden, 1985.

[58] J. Holmgren. Bolt-anchored, steel-fibre-reinforced shotcrete linings. *Tunneling and Underground Space Technology*, 2:319–333, 1987. doi: 10.1016/0886-7798(87)90043-5.

[59] J. Holmgren. *Design of shotcrete on soft drains in tunnels subjected to fluctuations in air-pressure from passing trains*. Technical report, Swedish Fortification Agency, Stockholm, Sweden, 1994.

[60] J. Holmgren. Shotcrete research and practice in Sweden: development over 35 years. In *Shotcrete elements of a system*, Sydney, Australia, 2010.

[61] K.G. Holter. Loads on sprayed waterproof tunnel linings in jointed hard rock: A study based on Norwegian cases. *Rock Mechanics and Rock Engineering*, 47(3):1003–1020, 2014. doi: 10.1007/s00603-013-0498-0.

[62] K.G. Holter. How do sprayed concrete linings with sprayed waterproof membranes function: Findings from a research project for traffic tunnels in hard rock in Norway. In *Proceedings of the 13th International Conference Underground Construction*, Prague, Czech Republic, 2016.

[63] K.G. Holter. Performance of EVA-based membranes for SCL in hard rock. *Rock Mechanics and Rock Engineering*, 49(4):1329–1358, 2016. doi: 10.1007/s00603-015-0844-5.

[64] K.G. Holter and S. Geving. Moisture transport through sprayed concrete tunnel linings. *Rock Mechanics and Rock Engineering*, 49(123):243–272, 2016. doi: 10.1007/s00603-015-0730-1.

[65] A.E. Indiart. *Coupled analysis of degradation process in concrete specimens at the meso-level*. Ph.D Thesis. Universitat Politécnica de Catalunya. Barcelona, Spain, 2009.

[66] H. Jalalifar and N. Aziz. Experimental and 3D numerical simulation of reinforced shear joints. *Rock Mechanics and Rock Engineering*, 43(1):95–103, 2010. doi: 10.1007/s00603-009-0031-7.

[67] R. Jansson. *Fire spalling of concrete theoretical and experimental studies*. Ph.D Thesis. KTH Royal Institute of Technology. Stockholm, Sweden, 2013.

[68] L. Kachanov. Time of rupture process under creep conditions. *Izvestiia Akademii Nauk SSSR*, 8:26–31, 1958.

[69] B. Lagerblad, L. Fjällberg, and C. Vogt. Shrinkage and durability of shotcrete. In *Shotcrete elements of a system*, pages 173–180, Sydney, Australia, 2010.

[70] M. Lato, M.S. Diederichs, D.J. Hutchinson, and R. Harrap. Optimization of LiDAR scanning and processing for automated structural evaluation of discontinuities in rockmasses. *International Journal of Rock Mechanics and Mining Sciences*, 46(1):194–199, 2009. doi: 10.1016/j.ijrmms.2008.04.007.

[71] C.K.Y. Leung, M. Asce, A.Y.F. Lee, and R. Lai. A new testing configuration for shrinkage cracking of shotcrete and fiber reinforced shotcrete. *Cement and Concrete Research*, 36(4):740–748, 2006. doi: 10.1016/j.cemconres.2005.11.018.

[72] C.C. Li, G. Kristjansson, and A.H. Høien. Critical embedment length and bond strength of fully encapsulated rebar rockbolts. *Tunnelling and Underground Space Technology*, 59:16–23, 2016. doi: 10.1016/j.tust.2016.06.007.

[73] U. Lindblom. *Time management of maintenance in rock tunnels for traffic*. Befo report 119, Rock Engineering Research Foundation, Stockholm, Swden, 2012.

[74] R. Malm. *Predicting shear type crack initiation and growth in concrete with non-linear finite element method*. Ph.D Thesis. KTH Royal Institute of Technology. Stockholm, Sweden, 2009.

[75] R. Malm. *Guideline for FE analyses of concrete dams*. Report 2016:270, Energiforsk, Stockholm, Sweden, 2016.

[76] L. Malmgren. *Interaction between shotcrete and rock*. Ph.D Thesis. Luleå University of Technology. Luleå, Sweden, 2005.

[77] L. Malmgren and E. Nordlund. Interaction of shotcrete with rock and rock bolts-A numerical study. *International Journal of Rock Mechanics and Mining Sciences*, 45(4):538–553, 2008. doi: 10.1016/j.ijrmms.2007.07.024.

[78] L. Malmgren, E. Nordlund, and S. Rolund. Adhesion strength and shrinkage of shotcrete. *Tunnelling and Underground Space Technology*, 20(1):33–48, 2005. doi: 10.1016/j.tust.2004.05.002.

[79] D. Mao, B. Nilsen, and L. Ming. Numerical analysis of rock fall at Hanekleiv road tunnel. *Bulletin of Engineering Geology and the Enviroment*, pages 783–790, 2012. doi: 10.1007/s10064-012-0438-3.

[80] D.R. Morgan. Advances in shotcrete technology for infrastructure rehabilitation. *Shotcrete Magazine*, 8(1):18–27, 2006.

[81] S. Myren, P. Hagelia, and O. Bjontegaard. The ban of polymer fibre in FRSC in Norwegian road tunnels. In *8th International Symposium on Sprayed Concrete*, Trondheim, Norway, 2018.

[82] J. Nemcik, S. Ma, N. Aziz, T. Ren, and X. Geng. Numerical modelling of failure propagation in fully grouted rock bolts subjected to tensile load. *International Journal of Rock Mechanics and Mining Sciences*, 71:293–300, 2014. doi: 10.1016/j.ijrmms.2014.07.007.

[83] M. Neuner, T. Cordes, M. Drexel, and G. Hofstetter. Time-dependent material properties of shotcrete : Experimental and numerical study. *Materials*, 10(1067):1–17, 2017. doi: 10.3390/ma10091067.

[84] B. Nilsen. Cases of instability caused by weakness zones in Norwegian tunnels. *Bulletin of Engineering Geology and the Environment*, 70:7–13, 2011. doi: 10.1007/s10064-010-0331-x.

[85] E. Nordström. *Durability of sprayed concrete*. Ph.D Thesis. Luleå University of Technology. Luleå, Sweden, 2005.

[86] NVT. *Tunnel linings*. Technical report, Nordisk Vegteknisk Forbund, Oslo, Norway, 2008.

[87] J. F. Olesen. Fictitious crack propagation in fibre-reinforced concrete beams. *Journal of Engineering Mechanics*, 127(3):272–280, 2001. doi: 10.1061/(ASCE)0733-9399(2001)127:3(272).

[88] J. Oliver, M. Cervera., S. Oller, and J. Lubliner. Isotropic damage models and smeared crack analysis of concrete. In *Proceedings of the 2nd International Conference on Computer Adided Analysis and Design of Concrete Strucutres*, pages 945–957, Zell am See, Austria, 1990.

[89] H. Ozturk. Fracture mechanics interpretation of thin spray-on liner adhesion tests. *International Journal of Adhesion and Adhesives*, 34:17–23, 2012. doi: 10.1016/j.ijadhadh.2012.01.001.

[90] H. Ozturk and D.D. Tannant. Thin spray-on liner adhesive strength test method and effect of liner thickness on adhesion. *International Journal of Rock Mechanics and Mining Sciences*, 47(5):808–815, 2010. doi: 10.1016/j.ijrmms.2010.05.004.

[91] H. Ozturk and D.D. Tannant. Influence of rock properties and environmental conditions on thin spray-on liner adhesive bond. *International Journal of Rock Mechanics and Mining Sciences*, 48(7):1196–1198, 2011. doi: 10.1016/j.ijrmms.2011.06.006.

[92] C.S.B. Paglia, F.J. Wombacher, and H.K. Böhni. Influence of alkali-free and alkaline shotcrete accelerators within cement systems: Hydration, microstructure, and strength development. *ACI Materials Journal*, 101(5): 353–357, 2004. doi: 10.14359/13420.

[93] D. Saiang, L. Malmgren, and E. Nordlund. Laboratory tests on shotcrete-rock joints in direct shear, tension and compression. *Rock Mechanics and Rock Engineering*, 38(4):275–297, 2005. doi: 10.1007/s00603-005-0055-6.

[94] J. Schlumpf, J. Höfler, and M. Jahn. *Sika sprayed concrete handbook 2011*. Technical report, Sika AG, Zurich, Switzerland, 2011.

[95] J. Silfwerbrand. Improving concrete bond in repaired bridge decks. *Concrete international*, 12(9), 1990.

[96] J. Silfwerbrand. Stresses and strains in composite concrete beams subjected to differential shrinkage. *ACI Structural Journal*, 94(4):347–353, 1997.

[97] J. Silfwerbrand. Bonded Concrete Overlays. *Concrete International*, (May): 1–19, 2017. doi: doi:10.1201/9781420007657.ch23.

[98] J.C. Simo and J.W. Ju. Strain and stress based continuum damage models I. Formulation. *International Journal of Solids and Structures*, 23(7):821–840, 1987. doi: 10.1016/0020-7683(87)90083-7.

[99] J.C. Simo and J.W. Ju. Strain and stress based continuum damage models II. Computational aspects. *Mathematical and Computer Modelling*, 12(3): 378, 1989. doi: 10.1016/0895-7177(89)90118-0.

[100] A. Sjölander. *Analyses of shotcrete stress states due to varying lining thickness and irregular rock surfaces*. Licentiate Thesis. KTH Royal Institute of Technology. Stockholm, Sweden, 2017.

[101] A. Sjölander and A. Ansell. Numerical simulations of restrained shrinkage cracking in glass fibre reinforced shotcrete slabs. *Advances in Civil Engineering*, 2017(1):11, 2017. doi: 10.1155/2017/8987626.

[102] A. Sjölander and A. Ansell. Investigation of non-linear drying shrinkage for end-restrained shotcrete of varying thickness. *Magazine of Concrete Research*, 70(6):271–279, 2018. doi: 10.1680/jmacr.17.00171.

[103] A. Sjölander and A. Ansell. In-situ and laboratory investigation on leaching and effects of early curing of shotcrete. *Nordic Concrete Research*, 61(2): 23–37, 2019. doi: 10.2478/ncr-2019-0014.

[104] A. Sjölander, R. Hellgren, and A. Ansell. Modelling aspects to predict failure of a bolt-anchored and fibre reinforced shotcrete lining. In *8th International Symposium on Sprayed Concrete*, Trondheim, Norway, 2018.

[105] A. Sjölander, A. Ansell, and R. Malm. In-situ and laboratory investigation on leaching and effects of early curing of shotcrete. *Tunnelling and Underground Space Technology*, 2020.

[106] A. Sjölander, R. Hellgren, R. Malm, and A. Ansell. Verification of failure mechanisms and design philosophy for a bolt-anchored and fibre-reinforced shotcrete lining. *Engineering Failure Analysis*, 116, 2020. doi: 10.1016/j.engfailanal.2020.104741.

[107] A. Sjölander, A. Nascetti, V. Belloni, and R. Ravanelli. TACK Project, 2020. URL `www.tackproject.xyz`.

[108] T. Soetens and S. Matthys. Different methods to model the post-cracking behaviour of hooked-end steel fibre reinforced concrete. *Construction and Building Materials*, 73:458–471, 2014. doi: 10.1016/j.conbuildmat.2014.09.093.

[109] M. Son. Adhesion strength at the shotcrete-rock contact in rock tunneling. *Rock Mechanics and Rock Engineering*, 46(5):1237–1246, 2013. doi: 10.1007/s00603-013-0380-0.

[110] K. Spang and P. Egger. Action of fully-grouted bolts in jointed rock and factors of influence. *Rock Mechanics and Rock Engineering 23*, pages 201–229, 1990. doi: 10.1007/BF01022954.

[111] R. Stacey. Review of membrane support mechanisms, loading mechanisms, desired membrane performance, and appropriate test methods. *The Journal of the South Africa Institute of Mining and Metallurgy*, 101(7):343–352, 2001. doi: 10.1007/BF01022954.

[112] H. Stille. Rock support in theory and practice. In *Proceedings of the international symposium on rock support*, Ontario, Canada, 1992.

[113] H. Stille and A. Palmström. *Rock engineering*. ICE Publishing, London, UK, 2010. ISBN 9780727740830.

[114] D.D. Tannant. Thin spray-on liners for underground rock support. In *Proceeding of the seventeenth International Mining Congress and Exhibition of Turkey*, Ankara, Turkey, 2001.

[115] P. Teichert. Carl Akeley, A tribute to the founder of shotcrete. *Shotcrete Magazine*, pages 10–12, 2002.

[116] A. Thomas. *Sprayed concrete lined tunnels*. Taylor & Francis, New York, USA, 2009. ISBN 0415368642.

[117] Trafikverket. *Design criterions for tunnels*. Technical report, Trafikverket, Borlänge, Sweden, 2016.

[118] Trafikverket. *Handbook for planning of tunnels*. Technical report, Trafikverket, Borlänge, Sweden, 2016.

[119] E.K. Tschegg and S.E. Stanzl. Adhesive power measurements of bonds between old and new concrete. *Journal of Materials Science*, 26(19):5189–5194, 1991. doi: 10.1007/BF01143212.

[120] E.K. Tschegg, H.M. Rotter, P.E. Roelfstra, U. Bourgund, and P. Jussel. Fracture mechanical behaviour of aggregate cement matrix interfaces. *Journal of Materials in Civil Engineering*, 7(4):199–203, 1995. doi: 10.1061/(ASCE)0899-1561(1995)7:4(199).

[121] M. Vandewalle. *Tunneling is an art*. N.V. Bekaert S.A, Zwevegem, Belgium, 2005.

[122] T. Wetlesen and B. Krutrök. Measurement of shotcrete thickness in tunnel with Bever 3D laser scanner operated from the robot. In *7th International Symposium on Sprayed Concrete*, Sandefjord, Norway, 2014.

[123] G.D. Yoggy. The history of shotcrete - Part 1. *Shotcrete Magazine*, pages 28–29, 2000.

[124] D.Y. Yoo, Y.S. Yoon, and N. Banthia. Predicting the post-cracking behavior of normal- and high-strength steel-fiber-reinforced concrete beams. *Construction and Building Materials*, 93:477–485, 2015. doi: 10.1016/j.conbuildmat.2015.06.006.

BeFo

Box 55545
SE-102 04 Stockholm

info@befoonline.org • www.befoonline.org
Visiting address: Sturegatan 11, Stockholm

ISSN 1104-1773